

HADRONS AND QCD INSTANTONS: A BOSONIZED VIEW

M. KACIR, M. PRAKASH AND I. ZAHED

Department of Physics
State University of New York at Stony Brook
Stony Brook, New York 11794-3800, USA

(Received October 13, 1998)

In a dilute system of instantons and antiinstantons, the $U_A(1)$ and scale anomalies are shown to be directly related to the bulk susceptibility and compressibility of the system. Using $1/N_c$ (where N_c is the number of colors) as a book-keeping argument, mesonic, baryonic and gluonic correlators are worked out in p -space and Fourier transformed to x -space for a comparison with recently simulated correlators. The results are in overall agreement with simulations and lattice calculations, for distances up to 1.5 fm, despite the fact that some channels lack the necessary physical singularities. We analyze various space-like form factors of the nucleon and show that they are amenable to constituent quark form factors to leading order in $1/N_c$. Issues related to the lack of confinement in the model and its consequence on the various correlation functions and form factors are also discussed.

PACS numbers: 12.38.Lg

1. Introduction

An outstanding problem in QCD is the understanding of the hadronic spectrum from first principles. Decades of dedicated lattice simulations have shown that the problem is difficult when all QCD degrees of freedom are taken into account. Through the years there have been numerous proposals, both theoretical and numerical, which suggest that only some relevant degrees of freedom may be important for the bulk aspects of the hadronic spectrum. The proposals range from lattice cooling procedures [1] to semi-classical techniques [2].

Recent lattice simulations based on cooling procedures have suggested that instanton and antiinstanton configurations may account for a large part of the hadronic correlations [3, 4], although the local character of the cooling algorithms may not totally rule out persistent quantum effects at large

distances [5]. On a periodic lattice (without twists), instanton or antiinstanton configurations are necessarily singular [6]. Their continuum analogs are the BPST instantons in singular gauge, a point of some recent concern [7]. Notwithstanding such concerns, an impressive amount of results, both from cooled lattice simulations [3, 4] and from random instanton simulations [8], seem to indicate that the basic features of the hadronic spectrum may emerge from a dilute ensemble of singular instantons and antiinstantons.

Sometime ago, 't Hooft's suggested [9] that instantons provide the answer to the axial $U_A(1)$ problem. In the presence of instantons or antiinstantons, light quarks acquire zero modes, which bunch into flavor-singlet configurations ('t Hooft's vertices) thereby dynamically breaking the axial $U_A(1)$ symmetry. At low energy, 't Hooft's interactions provide interesting correlations in various hadronic channels, as noted by Callan, Dashen and Gross [2], and analyzed using QCD sum rules [10], resummation procedures [12, 13], instanton simulations [14], and bosonisation techniques [15–18].

In this paper, we will assume that the QCD partition function simplifies into a grand canonical ensemble composed of 't Hooft's vertices, with an apriorily unspecified measure for the instanton-antiinstanton interactions. We will further assume that the ensemble is dilute with a screened topological charge, as discussed in Refs. [18–20]. The screening is expected from the feedback of the light quarks on the instantons and antiinstantons in the vacuum [21, 22]. In this respect, problems related to the original choice of the instanton-antiinstanton ansatz [23], as well as the limitations associated with the streamline approach [24], are somehow irrelevant. Analytical and numerical calculations with such an ensemble have led to a satisfactory phenomenology [8, 13, 19].

The purpose of this paper is to show that the analytically derived results using either resummation techniques [13] or bosonisation techniques [15, 19] for two and three flavors in momentum space, are consistent with the recent four-dimensional simulations [8] as well as with the cooled and quenched lattice simulations [4] up to a distance of 1.5 fm. At larger distances, the lack of confinement shows up in the form of spurious oscillations. The physics of a screened gas of instantons and antiinstantons is well described by simple mean field arguments [15, 19]. In Section 2, we recall the effective action for a random instanton gas using an approximate bosonisation scheme. In Section 3, we discuss the structure of the massive quark propagator both in momentum and coordinate spaces, and comment on heavy–light correlators. We note that in the long wavelength limit, the quark propagator becomes tachyonic for all current quark masses. In Section 4, we outline the result for the quark condensate in the random instanton gas. In Section 5, we give a brief account of the various mesonic correlators, including the scalars. We discuss issues related to the mixing between the scalars and

the fluctuations in the instanton scalar density through the scale anomaly. The mixing between the pseudoscalar singlet and the fluctuations in the instanton pseudoscalar density yields naturally to a resolution of the $U_A(1)$ problem. Issues related to the $\eta - \eta'$ mixing are also discussed. The p -space results are discussed in detail for scalars, pseudoscalars and vectors, and compared with the x -space simulations. While the analysis of the p -space pseudoscalar correlator shows clear evidence of poles, the vector correlators simply exhibit two constituent quarks. In Section 6, we briefly discuss non-strange baryons in x -space. In Section 7, scalar and pseudoscalar gluonic correlation functions are discussed. In Section 8, quark and gluon form factors of the constituent quark are discussed. To leading order in $1/N_c$, they saturate the nucleon form factor following from the point-to-point correlator in terms of Ioffe's current. Our conclusions and recommendations are summarised in Section 9.

The details of the bosonisation techniques are given in Appendix A. In Appendix B, we provide a direct calculation of the quark condensate. In Appendix C, the necessary elements for a Gaussian approximation are presented. In Appendix D, the effective action for the singlet and octet pseudoscalars is explicitly worked out. In Appendix E, an extension bosonization scheme is presented. In Appendix F, the various expressions entering the unconnected parts of the mesonic correlators are summarized. Some of the difficulties related with the expansion of the mesonic vertices involving the strange quark mass are discussed in Appendix G. In Appendix H, we outline the essentials of our numerical procedures.

2. Model

• Effective action

't Hooft has shown that at scales larger than a typical instanton size ρ (fixed throughout this paper), instantons induce flavor mixing between the light u, d and s quarks in the form of determinantal interactions ('t Hooft determinants) [9]

$$\det_{\pm} = \frac{1}{N_f!} \det_{fg} \left(m^{fg} \rho - \frac{\rho}{2i} \left\langle \int \psi^{\dagger f} S_0^{-1} \phi^{\pm} \int \phi^{\pm \dagger} S_0^{-1} \psi^g \right\rangle \right), \quad (1)$$

where $m^{fg} = \text{diag}(m, m, m_s)$ is the current mass matrix for (u, d, s) quarks, ϕ_{\pm} are the instanton–antiinstanton zero modes, ψ is the fermion field in the long wavelength limit, and $S_0^{-1} = -(i\cancel{\partial} + im)$ is the free fermion propagator. The averaging implied by $\langle \dots \rangle$ is over the instanton and antiinstanton color orientations.

A random system of instantons and antiinstantons that is compatible with the $U_A(1)$ and scale anomaly yields the generating functional [9, 17, 20]

$$Z[\eta, \eta^\dagger] = \int dn_+ dn_- \mathcal{D}\psi \mathcal{D}\psi^\dagger \mu(n_+, n_-) e^{-\int d^4z \mathcal{L}[\eta, \eta^\dagger, n_+, n_-]}, \quad (2)$$

where

$$\mathcal{L}[\eta, \eta^\dagger, n_+, n_-] = \psi^\dagger S_0^{-1} \psi - n_+ \log \det_+ - n_- \log \det_- - \psi^\dagger \eta - \eta^\dagger \psi \quad (3)$$

in (2) at the saddle points. Throughout this paper, the generating functional will be used to carry calculations to leading order in $1/N_c$, where N_c counts the number of colors. The counting will be understood just as a convenient way of organizing the calculation, with $N_c = 3$. In the presence of instantons, conventional N_c arguments have to be amended [25] (see also below).

We are using a coarse grained action for the description of the instantons and antiinstantons, as discussed in [20]. The relation to the uncoarse-grained approach, follows from the identification

$$n^\pm(z) = \pm \sum_{i=1}^{N_\pm} \delta^4(z - z_i) \quad (4)$$

at the saddle points ($N_c = 3 \gg 1$). The coarse grained version highlights the role of the scalar and pseudoscalar glueball fields, and their mixing to the quark–antiquark excitations. The measure $\mu(n_+, n_-)$ refers to the distribution of instantons and antiinstantons in the vacuum without the quarks (quenched approximation). Its form is generic, and follows solely from the $U_A(1)$ and scale anomalies [20]

$$\mu(n_+, n_-) = \exp\left(-\frac{n}{\sigma_*^2} \int d^4z (n^+(z) + n^-(z)) \left(\log \frac{n^+(z) + n^-(z)}{n} - 1 \right) - \frac{1}{2\chi_*} \int d^4z (n^+(z) - n^-(z))^2 \right), \quad (5)$$

where $n = N/V_4 \sim N_c$ is the mean instanton and antiinstanton density in the thermodynamical limit, $\chi_* = n \sim N_c$ [23] the quenched topological susceptibility

$$\chi_* = \left\langle \left(\int d^4z (n_+ - n_-)(z) \right)^2 \right\rangle_{N_f=0} \quad (6)$$

and σ_* the quenched compressibility ($a = 1, 2, \dots$)

$$\left(\frac{\sigma_*^2}{n} \right)^{a-1} = \frac{1}{N} \left\langle \left(\int d^4z (n^+ + n^- - n)(z) \right)^a \right\rangle_{N_f=0}. \quad (7)$$

- Anomalies

The coarse grained effective action (3) along with the measure (5) satisfies both the axial U(1) and scale anomaly [20]. Indeed, in the chiral limit the determinants in (2) acquire a phase under a U(1) axial rotation, hence a non-conserved axial-singlet current,

$$\partial_\mu j_{\mu 5}(z) = 2N_f(n_+ - n_-)(z) + 2i \text{Tr}_f m \psi^\dagger(z) \gamma_5 \psi(z). \quad (8)$$

Also, in the quenched approximation, the measure (5) is not scale invariant. As a result, the divergence of the dilatational current (trace of the energy momentum tensor $\Theta_{\mu\nu}$), is not conserved,

$$\Theta_{\mu\mu}(z) = \frac{4n}{\sigma_*^2} (n^+(z) + n^-(z)) + \frac{2}{\chi_*} (n_+(z) - n_-(z))^2 + \mathcal{O}(N_f). \quad (9)$$

Comparison with the QCD form of the trace anomaly [26] gives $\sigma_*^2/n \sim 12/11N_c \sim 1/N_c$.

In the fermionic part, we note that for $n_+ = n_-$, the generating functional (2) involves only the combination $(\det_+ \det_-)$ and is invariant under $U_L(3) \times U_R(3)$. The fluctuations in $(n^+ + n^-)$ involve mixing between the isosinglet scalar and the scalar “glueballs”, through

$$-\frac{1}{2} \int d^4z (n^+ + n^-)(z) \ln \left(\det_+ \times \det_- \right). \quad (10)$$

For $n_+ \neq n_-$, the combination (\det_+/\det_-) is also allowed. The latter dynamically breaks the axial U(1) symmetry through

$$-\frac{1}{2} \int d^4z (n^+ + n^-)(z) \ln \left(\frac{\det_+}{\det_-} \right) \quad (11)$$

as originally suggested by 't Hooft. The fluctuations in $(n^+ - n^-)$ will mix with the isosinglet pseudoscalar, thereby resolving the $U_A(1)$ problem (see below).

- Bosonization

In vacuum, the packing fraction is given by the dimensionless combination

$$n_* \rho^4 = \frac{n}{2N_c} \rho^4 \sim 10^{-3}. \quad (12)$$

Since the density $n \sim N_c$, the packing fraction is of order N_c^0 . The value (12) is small, and an expansion in the density is justified except in the presence of

infrared singularities, as we will specify below. In this spirit, the generating functional (2) can be bosonized approximately by inserting the identity ¹

$$\mathbf{1} = \int \mathcal{D}\pi^\pm \mathcal{D}P^\pm \exp \left(\text{Tr}_f \int dk dl P^\pm(k, l) \left(\pi^\pm(k, l) - \theta^\pm(k, l) \right) \right) \quad (13)$$

in the partition function (2), where π^\pm and P^\pm are bilocal auxiliary fields and $N_f \times N_f$ valued such that $P^\pm(k, l) = P^\pm(k-l)$ and similarly for $\pi^\pm(k, l)$. Also (see Appendix A)

$$\theta^\pm(k, l) = \langle \psi^\dagger(k) S_0^{-1} \phi^\pm(k) \phi^{\pm\dagger}(l) S_0^{-1} \psi(l) \rangle. \quad (14)$$

The trace over flavor indices is understood in the exponent (13). The auxiliary fields π^\pm can be eliminated by using the saddle point approximation. From Appendix A, we have

$$Z[\eta, \eta^\dagger] = \int \mathcal{D}P^\pm e^{-\eta^\dagger \mathcal{S}[P^+, P^-] \eta} e^{-S_{\text{eff}}(P^\pm)}, \quad (15)$$

where the effective action is given by

$$\begin{aligned} S_{\text{eff}}(P^\pm) &= -N_c \text{Tr}(\log \mathbf{S}^{-1}[P^+, P^-]) \\ &+ \frac{n}{2} \int dz \left(\text{Tr} \ln \frac{4}{n\rho} P^+(z) + \text{Tr} \ln \frac{4}{n\rho} P^-(z) \right) \\ &- 2 \int dz \text{Tr}_f m(P^+(z) + P^-(z)). \end{aligned} \quad (16)$$

The trace Tr is over flavor and Dirac indices as well as four momenta, the Tr_f over flavor indices and the \det is over flavor indices as well position space. We have explicitly used ² $n_+ = n_- = n/2$ and defined the operator momentum dependent inverse propagator

$$\begin{aligned} \mathbf{S}^{-1}[P^+, P^-] &= \hat{k} - im - i\sqrt{M_k} \\ &\times \left(1 - i \frac{m\hat{k}}{k^2} \right) (P^+ \gamma_5^+ + P^- \gamma_5^-) \left(1 - i \frac{m\hat{k}}{k^2} \right) \sqrt{M_k}. \end{aligned} \quad (17)$$

Here, \hat{k} refers to the momentum operator and M_k is the induced momentum dependent screening quark mass. The screening mass arises from averaging over the instanton zero modes [13]. From Appendix C, we have after

¹ In what follows, we use the shorthand notation $dk = d^4k/(2\pi)^4$ and $dz = d^4z$ when integrating.

² This constraint will be relaxed below to address the η' mass and the gluon correlators.

rescaling

$$M_k = M_k(m) = \lambda(m) \frac{n}{N_c} k^2 \phi'^2 = \lambda(0) \frac{n}{N_c} k^2 \left(\pi \rho^2 \frac{d}{d\tau} (I_0 K_0 - I_1 K_1) \right)^2, \quad (18)$$

where $\tau = k\rho/2$ is the argument of the McDonald functions I and K . From (16) and (17) it follows that in the long wavelength limit quarks in the instanton vacuum interact via the exchange of effective bosonic fields P^\pm . The latter are $N_f \times N_f$ valued and may be parametrized as

$$P^\pm = e^{\pm \frac{1}{2} i \kappa} \sigma e^{\pm \frac{1}{2} i \kappa}. \quad (19)$$

Other parametrizations are also possible [27]. We note, however, that to the order we will discuss the correlation functions below (Gaussian approximation), the results are parametrization independent.

- Gap equation

The matrices κ and σ are $N_f \times N_f$ valued and hermitean. The κ variables can be identified as the pseudoscalar Goldstone modes, except for κ_0 . The matrix σ contains the massive scalar–isoscalar and scalar–isovector excitations. The non zero value of σ in the vacuum follows from the saddle point approximation to (16) by setting $\kappa = 0$, and switching off the sources. The result is an integral equation for each flavor

$$1 - 2m\lambda(m) = 4 \frac{N_c}{n} \int \frac{d^4 k}{(2\pi)^4} \frac{(k^2 + m^2) M_k^2(m) - m M_k(m) k^2}{k^4 - 2m M_k(m) k^2 + (k^2 + m^2) M_k^2(m)}, \quad (20)$$

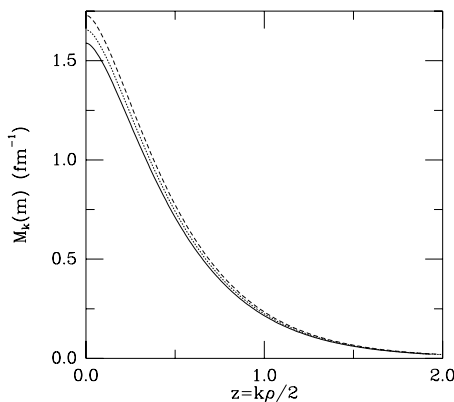


Fig. 1. The constituent quark mass $M_k(m)$ versus $z = k\rho/2$ (k being the momentum and ρ the average size of the pseudoparticle) for current masses $m = 0$ (dashed curve), $m = 5$ MeV (dotted curve) and $m = 10$ MeV (solid curve), respectively.

where we have set $M_k(m)/M_k(0) = \lambda(m)/\lambda(0)$. For an instanton density $n = 1 \text{ fm}^{-4}$ and size $\rho = 0.33 \text{ fm}$, the behaviour of the constituent quark mass $M_k(m)$ versus the dimensionless combination $z = k\rho/2$ is shown in Fig. 1 with current quark masses $m = 0$ (dashed), 5 MeV (dotted) and 10 MeV (solid), respectively. For $k \rightarrow 0$, $M_0(m) \rightarrow \lambda(m) (n/N_c)(2\pi\rho)^2$, while for $k \gg 1$, $M_k(m)$ falls off like $1/k^6$. The width at half maximum is of order $1/\rho$. The result (20) was also obtained in [28] using different arguments.

3. Quark propagator

In a random instanton gas, quarks are “screened”. The light fermion propagator acquires a momentum dependent mass³. For one flavor, the results of Appendix A give (unless specified, we denote $M_k(m)$ by M_k)

$$S(k, m) = \frac{1}{\not{k} - im} - \frac{1}{\not{k} - i(m - k^2/M_k)}. \quad (21)$$

In the massless case [13]

$$S(k, 0) = \frac{1}{\not{k} - iM_k(0)}. \quad (22)$$

We note, however, that at low momentum, $M_k(m)$ acquires a non-analytical contribution ($k \rightarrow 0$)

$$M_k(m) \sim M_0(m) \left(1 + 3z^2 \log \frac{z}{2} e^{c+\frac{1}{2}} \right)_{z=k\rho/2}, \quad (23)$$

where $c = 0.577$ is Euler’s constant. The screening mass $M_0(m)$ does not show up as a simple pole. What this means is that, as $k \rightarrow 0$, the screened quarks become tachyonic. To the extent that long wavelength quarks are unphysical, this should be of no real concern. However, since the instanton model does not provide for confinement, these “unphysical” effects will contaminate all large distance behaviours. The instanton simulations [8], or cooled lattice calculations [4] have not probed large distances.

With this in mind, we now proceed to x -space with the decomposition

$$S(x, m) = S_0(x, m) + S_1(x, m), \quad (24)$$

where $S(x, m)$ is the Fourier transform of (21) and

$$S_0(x, m) = \frac{im^2}{4\pi^2} \left(\frac{\not{x}}{x^2} K_2(mx) + \frac{1}{x} K_1(mx) \right) \quad (25)$$

³ In general, the quark propagator is gauge dependent. Our case is no exception, and the present discussion should be understood as the evaluation of the quark propagator in a random and classical background of instantons and antiinstantons in a singular gauge.

is the free propagator of quark of mass m . $S_1(x, m)$ follows from (24) and will be understood as

$$S_1(x, m) = i \left(\not{x} S_1^{\text{odd}} - S_1^{\text{even}} \right) (x, m), \quad (26)$$

where

$$S_1^{\text{odd}}(x, m) = \frac{1}{x} \frac{\partial}{\partial x} \left(\frac{1}{4\pi^2 x} \int_0^{+\infty} dk \frac{k^2}{k^2 + (m - k^2/M_k)^2} J_1(kx) \right) \quad (27)$$

and

$$S_1^{\text{even}}(x, m) = \frac{1}{4\pi^2 x} \int_0^{+\infty} dk \frac{k^2(m - k^2/M_k)}{k^2 + (m - k^2/M_k)^2} J_1(kx). \quad (28)$$

Figs 2(a) and 2(b) show the behaviour of $m\text{Tr}S(x, m)/\text{Tr}S_0(x, m = 0)$ (chirality flip) and $\text{Tr}\gamma_4 S(x, m)/\text{Tr}\gamma_4 S_0(x, m = 0)$ (chirality non-flip) *versus* x up to 2 fm, for quark masses of 5 MeV (lower curve) and 10 MeV (upper curve), respectively. The squares refer to the results of simulations of Ref. [8] using 128 instantons and 128 antiinstantons in a periodic Euclidean box of $3.36^3 \times 6.72 \text{ fm}^4$. These simulations were carried out with equal u and d quark masses of $m = 10 \text{ MeV}$. The small discrepancy in the chirality flip part of the propagator may be due to the fact that the instanton simulations make explicit use of the single-instanton distorted propagator for the nonzero mode part, while the bosonized constructions presented above make use of the undistorted light quark propagator for the nonzero mode part.

Figs 2(c) and 2(d) show the chirality flip and non-flip part of the quark propagator for $m_u = 10 \text{ MeV}$ and $m_s = 140 \text{ MeV}$ over a wider range of x . The larger the quark mass, the larger the oscillation in the quark propagator at large distances. These spurious oscillations are due to the appearance of the tachyonic mass (23) and the occurrence of the combination $(m - k^2/M_k)$ in the quark propagator, and will cause most correlators to lack scaling at large distances (typically of the order of 2.5 fm and larger) as we will discuss below. We have checked that these oscillations persist in the massless case. In fact for $m = 0$ Fig. 2(c) is almost unchanged.

At this stage, we should point out that our treatment of the current masses is only approximate, given our definitions (1) and (2). We will check below that the linear effects in the current mass do reproduce known results, while the non-linear effects cancel out at large distances, leaving us with the expected masses for the strange pseudoscalars. Similar observations apply to the instanton simulations in [8], although the handling of the current masses is not necessarily the same as the one discussed here.

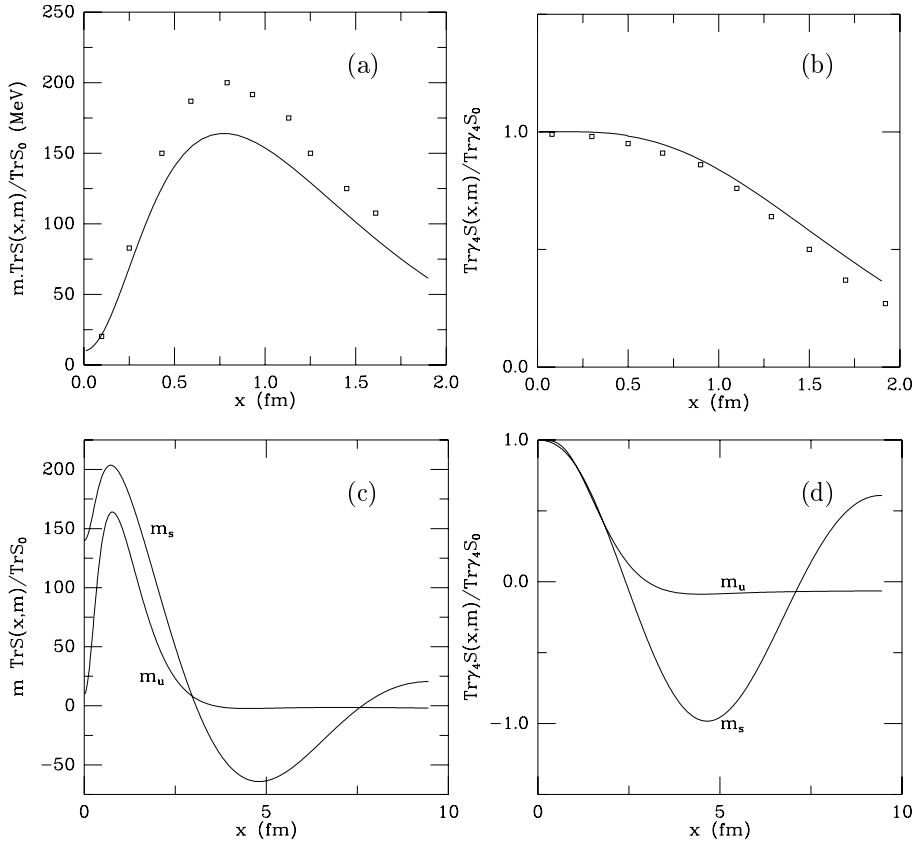


Fig. 2. The chirality flip (a) and non-flip (b) parts of the quark propagator (normalized to the free massless quark propagator) *versus* x (fm) for current masses of 5 MeV (lower curve) and 10 MeV (upper curve), respectively. The squares are results of simulations carried out in [8] for 128 instantons and 128 antiinstantons in a periodic box. The large distance behaviours are also shown for the chirality flip (c) and chirality non-flip parts (d).

Finally, we note that the naive interpretation that the x -space version of $\text{Tr}(S(x, m)(1 \pm \gamma_4)/2)$ as the correlator of a light quark in the field of an infinitely heavy quark [8, 29] overlooks the issue of binding. As it stands, the non-relativistic projection of the heavy-light-propagator without the Wilson line (Coulomb field) for the heavy particle reflects solely on a screened light quark. In a heavy-light system like a D or B meson, the light quark is expected to bind to the heavy source, causing the spectral function to develop a pole instead of a cut. A detailed analysis of systems with few heavy and light quarks in a random instanton gas has been given in Ref. [30].

In the Coulomb field of a heavy quark, the light quarks bind with a binding energy of the order of a quarter of the screening mass [30].

4. Quark condensate

The formation of a quark condensate in the instanton vacuum follows from the random nature of the system. From our bosonized construction, the quark condensate is obtained from the effective action (16) through

$$\langle \bar{\psi}\psi \rangle = \frac{1}{V_4} \frac{\partial S_{\text{eff}}[0, 0]}{\partial m}. \quad (29)$$

Since the present treatment is semi-classical, all the ambiguities associated with the current mass singularities are ignored. At the saddle point, a straightforward calculation in the $m \rightarrow 0$ limit gives

$$\begin{aligned} \langle \bar{\psi}\psi \rangle = & -4N_c \left(\frac{n}{2N_c} \lambda(0) - \int dk \frac{M_k}{(k^2 + M_k^2)} \right) \\ & - \frac{\lambda'(0)}{\lambda(0)} \left(4N_c \int dk \frac{M_k^2}{k^2 + M_k^2} - n \right). \end{aligned} \quad (30)$$

Using the mass gap equation for zero current mass, the term in brackets multiplying $\lambda'(0)$ vanishes and we are left with

$$\langle \bar{\psi}\psi \rangle = -4N_c \left(\frac{n}{2N_c} \lambda(0) - \int \frac{d^4 k}{(2\pi)^4} \frac{M_k}{(k^2 + M_k^2)} \right). \quad (31)$$

As a check, we show in Appendix B how this result can be recovered from the original definition in the saddle point approximation, prior to the bosonisation procedure. Numerically⁴,

$$\frac{n}{2N_c} \lambda(0) = 2 \int \frac{d^4 k}{(2\pi)^4} \frac{M_k}{(k^2 + M_k^2)} \quad (32)$$

so that

$$\langle \bar{\psi}\psi \rangle = -4N_c \int \frac{d^4 k}{(2\pi)^4} \frac{M_k}{(k^2 + M_k^2)} = -\langle S(0, m \rightarrow 0_+) \rangle \quad (33)$$

which is the expected result to leading order in $1/N_c$.

⁴ With our choice of parameters, the discrepancy is (10) MeV³.

5. Mesonic correlators

To leading order in $1/N_c$, the mesonic correlation functions follow from (16) by differentiation with respect to the external sources in the presence of the auxiliary bosonic fields P^\pm . Generically,

$$C_\gamma(x) = \langle T^* \psi^\dagger \gamma \psi(x) \psi^\dagger \gamma \psi(0) \rangle \tag{34}$$

with $\gamma = (1, \gamma_5, \gamma_\mu, \gamma_5 \gamma_\mu, \sigma_{\mu,\nu}) \otimes (1, T^a)$. From (16) we have $C_\gamma = C_\gamma^0 + C_\gamma^1$, where the connected part of the correlator is given by

$$C_\gamma^0(x) = -\frac{1}{Z[0, 0]} \int DP^\pm \text{Tr} (\mathbf{S}[x, 0; P] \gamma \mathbf{S}[0, x; P] \gamma) e^{-S_{\text{eff}}[P^\pm]} \tag{35}$$

and the unconnected part is given by

$$C_\gamma^1(x) = \frac{1}{Z[0, 0]} \int DP^\pm \text{Tr} (\mathbf{S}[x, x; P] \gamma) \text{Tr} (\mathbf{S}[0, 0; P] \gamma) e^{-S_{\text{eff}}[P^\pm]}. \tag{36}$$

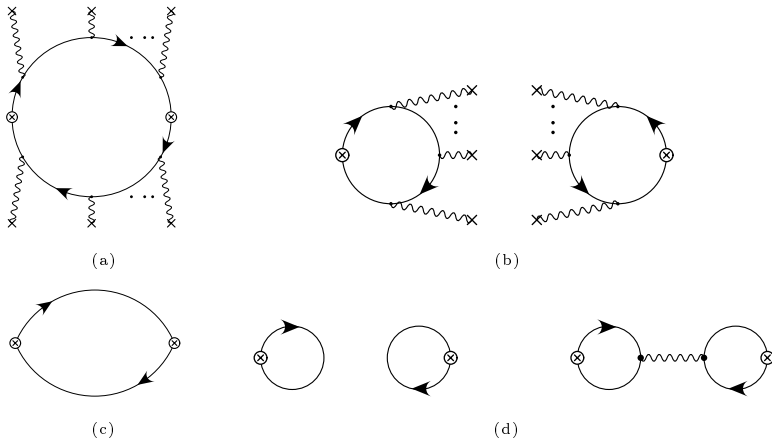


Fig. 3. The connected (a) and unconnected (b) parts of the correlator with arbitrary quantum numbers. The insertions correspond to the external background field P^\pm as discussed in the text. The resulting connected (c) and unconnected (d) parts to leading order in $1/N_c$ counting.

Typical diagrams contributing to (34) are shown in Figs 3(a) and 3(b). Only the diagrams in Figs 3(c) and 3(d) are dominant. They will be the only ones discussed here. In p -space, the contribution of Fig. 3(c) is

$$C_\gamma^0(p) = -N_c \int \frac{d^4k}{(2\pi)^4} \text{Tr} (S(1) \gamma S(2) \gamma) , \tag{37}$$

where $S(1, 2) = S(k \pm p/2, m_{1,2})$ for two arbitrary flavors. This contribution in the long wavelength limit reflects on the lack of confinement in the model. The contribution of Fig. 3(d) is

$$C_\gamma^1(p) = \frac{N_c}{2} \sum_{\pm} \frac{(R_\gamma^\pm(p) \pm R_\gamma^\mp(p)) (R_\gamma^\pm(-p) \pm R_\gamma^\mp(-p))}{\Delta_\pm(p)}. \quad (38)$$

The extraction of Δ_\pm and R_\pm from (16) is performed in Appendices B and C, respectively. With the above approximation in mind, the total correlation function reduces to the sum of (37) and (38), *i.e.* $C_\gamma = C_\gamma^0 + C_\gamma^1$. The results (37)–(38) were first derived by Dyakonov and Petrov for two massless flavors using detailed resummation procedures [13].

At this stage, it is interesting to compare the expression we have for the mesonic correlator in the instanton model with the one derived in planar QCD₂. In the large N_c limit, the two-fermion cut in QCD₂ is infrared sensitive and cancels exactly against the infrared sensitive one-gluon exchange graph [31]. This cancellation makes explicit use of Ward identities in Feynman graphs. It is essentially quantum and thus absent from the present semiclassical argument. The lack of confinement in our case will have dramatic consequences on the large distance behavior of the various correlation functions as we will discuss below.

The expressions used to generate the various correlators in p -space are tabulated in Appendix D. In Figs 4, we show the behaviour of the connected (minus the vacuum) correlators in the various channels *versus* the momen-

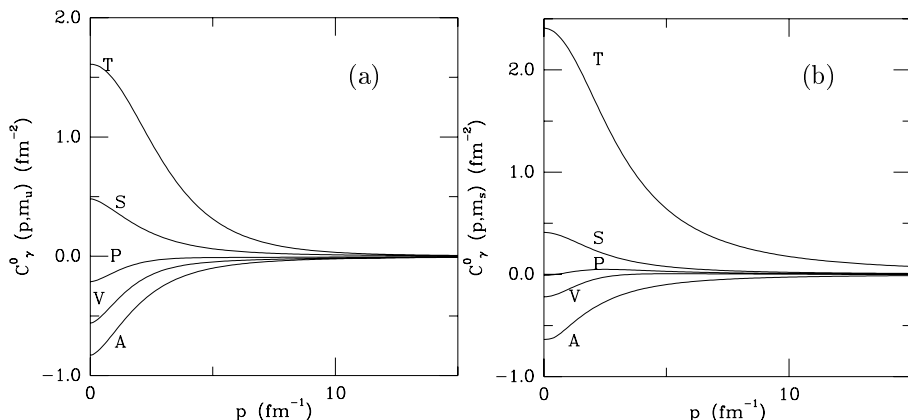


Fig. 4. The connected part $C_\gamma^0(p)$ of the correlator (normalized to the free and massless correlator). (a) for the up (down) quark ($m_u = m_d = 10$ MeV), and (b) for the strange quark ($m_s = 140$ MeV) *versus* p (fm^{-1}). The channels shown are scalar (S), pseudoscalar (P), vector (V), tensor (T) and axial-vector (A), respectively.

tum p , for the Axial- (A), Vector- (V), Pseudoscalar- (P), Scalar- (S) and Tensor-channel (T), without strangeness (Fig. 4(a)) and with strangeness (Fig. 4(b)). Similar correlators are shown in Figs 5 for the unconnected part. By about $p \sim 10 \text{ fm}^{-1}$ the correlations are totally washed out. The plots are for u and d quark masses of 10 MeV and a strange quark mass of 140 MeV. Although unconventional, this choice of the current masses allow for a comparison with the numerical simulations of Ref. [8].

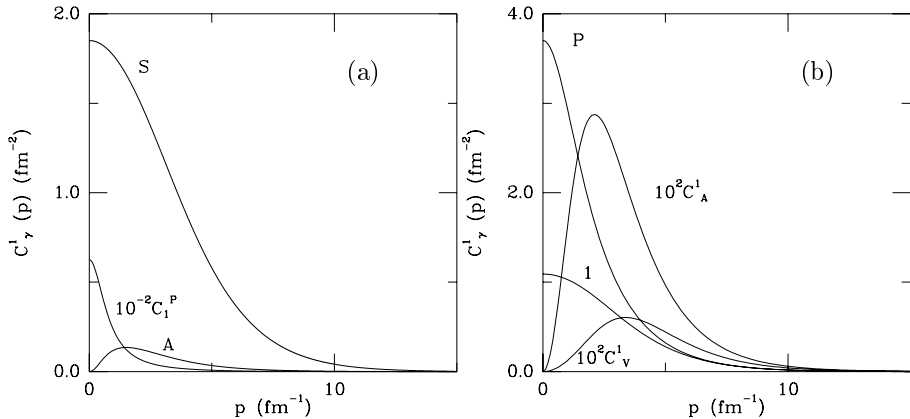


Fig. 5. The same as in Figs 4 but for the unconnected part $C_\gamma^1(p)$ of the correlator. The tensor channel vanishes identically for the up and strange quarks as does the vector channel for the up quark.

5.1. Gell-Mann–Oakes–Renner relation

In the pion channel, a pole is produced by the unconnected part of the correlator that lies well below the two-constituent quark cut. This is a good example of an infrared sensitive channel, where a simple expansion in the instanton density fails. The presence of small denominators through zero modes forces the resummation of an infinite string of terms of increasing powers in the instanton density, causing the correlation function to develop a pole. Using the small momentum expansion (see Appendix F), we have in the pseudoscalar channel

$$\Delta_-(p) = \frac{f^2}{4N_c} (M_-^2 + p^2 + \mathcal{O}(m^2, p^2)) \quad (39)$$

to leading order in the current quark mass m . Above, the decay constant f satisfies

$$f^2 = 4N_c \int \frac{d^4k}{(2\pi)^4} \frac{M_k^2 - \frac{k}{2}M'_k + \frac{k^2}{4}M_k'^2}{(k^2 + M_k^2)^2} \quad (40)$$

and the pseudoscalar mass M_- is given by

$$\frac{f^2}{4N_c} M_-^2 = 2m \left(\frac{n}{2N_c} \lambda(m) - \int \frac{d^4k}{(2\pi)^4} \frac{M_k}{k^2 + M_k^2} \right). \quad (41)$$

To this order, the quark condensate is current mass independent and is given by (31). Thus,

$$f_\pi^2 m_\pi^2 = -2m \langle \bar{\psi}\psi \rangle \quad (42)$$

which is the current algebra result derived by Gell-Mann, Oakes and Renner (GOR) [32]. For equal u and d quark masses with $m = 5$ MeV, we obtain $m_\pi = 158$ MeV, $\langle \bar{\psi}\psi \rangle = -(249 \text{ MeV})^3$ and to leading order in the current mass $f_\pi = 88$ MeV. Similar results can be derived for K and η , although the small momentum expansion is no longer valid for the unconnected part of the correlation function with a large strange quark mass. This point is further discussed in Appendix F.

In the expansion discussed above, the consistency of the GOR result can be further checked by noting that the unconnected part in the pion channel reads

$$C_\pi^1(p \sim 0) = \frac{1}{2} \left(\frac{4N_c}{f_\pi} R_\pm^{\gamma_5}(0) \right)^2 \frac{1}{p^2 + m_\pi^2}, \quad (43)$$

where

$$R_\pm^{\gamma_5}(0) = -2 \int \frac{d^4k}{(2\pi)^4} \frac{M_k}{k^2 + M_k^2}. \quad (44)$$

The term in brackets in the expression for C_π^1 can be identified with the usual pseudoscalar strength g_π . From (31)–(33), it follows that $g_\pi \sim 2 \langle \bar{\psi}\psi \rangle / f_\pi$.

5.2. Pseudoscalars

• π and K

Figs 6 and 7 show the behaviour of the pion and kaon correlators *versus* x , respectively, as they follow from (37) and (38) by Fourier transforms. The upper curve is for $m = 5$ MeV, while the lower curve is for $m = 10$ MeV. The squares are the results of simulations using 128 instantons and 128 antiinstantons in a $(3.36^3 \times 6.72)$ fm⁴ periodic box. The dotted circles are the results from cooled and quenched lattice gauge calculations on a $16^3 \times 24$ lattice with a physical lattice spacing of 0.17 fm.

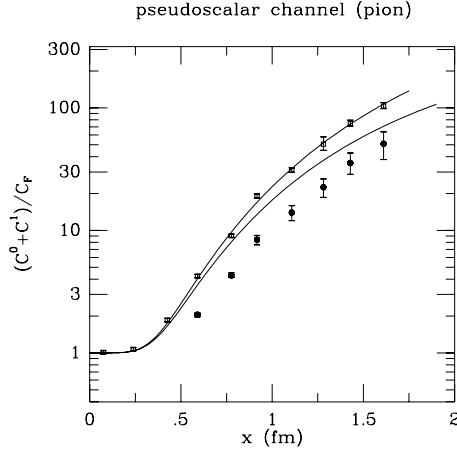


Fig. 6. The pion-correlator (normalized to the free and massless correlator) *versus* x (fm) for $m_u = m_d = 5$ MeV (upper curve) and $m_u = m_d = 10$ MeV (lower curve). The squares are the results obtained in [36] using 128 instantons and 128 antiinstantons in a periodic box. The circles are the results obtained in [4] from cooled lattice gauge calculations.

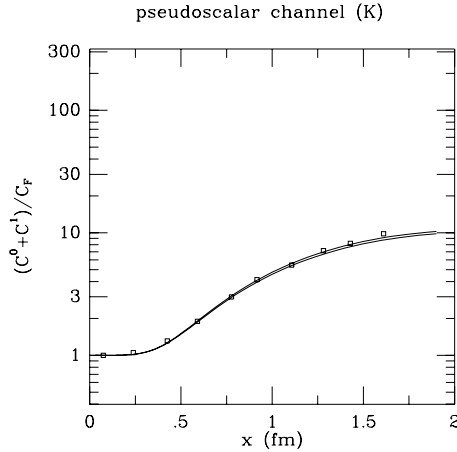


Fig. 7. The kaon-correlator (normalized to the free and massless correlator) *versus* x (fm) for $m_u = m_d = 5$ MeV (upper curve) and for $m_u = m_d = 10$ MeV (lower curve). The squares are the results obtained in [36] using 128 instantons and 128 antiinstantons in a periodic box.

The momentum dependent parts display a low-lying spurious cut at about 627 MeV, as well as a pole in the scalar and pseudoscalar channels. In Fig. 8, we display these two separate contributions to the pion channel for an average quark mass of 10 MeV.

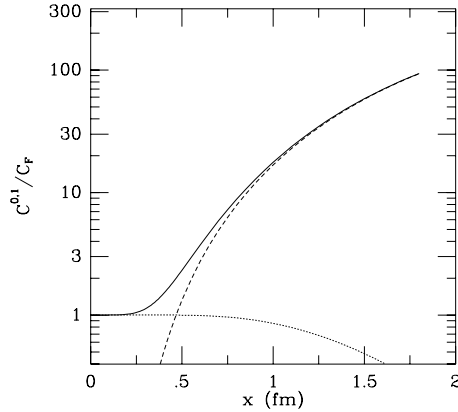


Fig. 8. In the pion channel, the connected $C^0(x, m_u)$, unconnected $C^1(x, m_u)$ and full correlators for $m_u = 10$ MeV *versus* x (fm) are plotted in dashed, dotted and solid lines, respectively.

The asymptotic form of the correlation function in x -space is strongly influenced by the position of the pole in most channels. Indeed, the large distance behaviour produced by the pole is approximately of the form

$$C_\gamma^1(x \rightarrow \infty) \simeq \frac{(gM_\pm)^2}{4} \frac{e^{-M_\pm x}}{(2\pi M_\pm x)^{3/2}} \quad (45)$$

which is to be compared with the contribution of two “regular” (not tachyonic) screened quarks:

$$C_\gamma^0(x \rightarrow \infty) \simeq \frac{N_c}{4} M_0^6 \frac{e^{-2M_0 x}}{(2\pi M_0 x)^3} \left(\text{Tr}(\gamma\gamma) - \frac{\text{Tr}(\not{x}\gamma\not{x}\gamma)}{x^2} \right) \quad (46)$$

with $M_0 = M_0(m)$. Beyond 2 fm, the running mass $(m - k^2/M_k)$ causes (46) to oscillate as shown in Figs 9 and 10. These oscillations, however, are overpowered in the pion channel given the very large signal caused by the pion pole compared to the spurious cut (about 100 : 1). We note that for $m = 10$ MeV, the screening mass for the two screened quarks is about 627 MeV. In (45), the pseudoscalar mass squared M_-^2 follows from the GOR relation

$$M_-^2 = -(m_1 + m_2) \frac{\langle \bar{\psi}\psi \rangle}{f^2}. \quad (47)$$

In the case of the pion, we plot in Fig. 11 the total correlator times $x^{3/2}$ for quark masses of 5 and 10 MeV, respectively. The pion mass sets

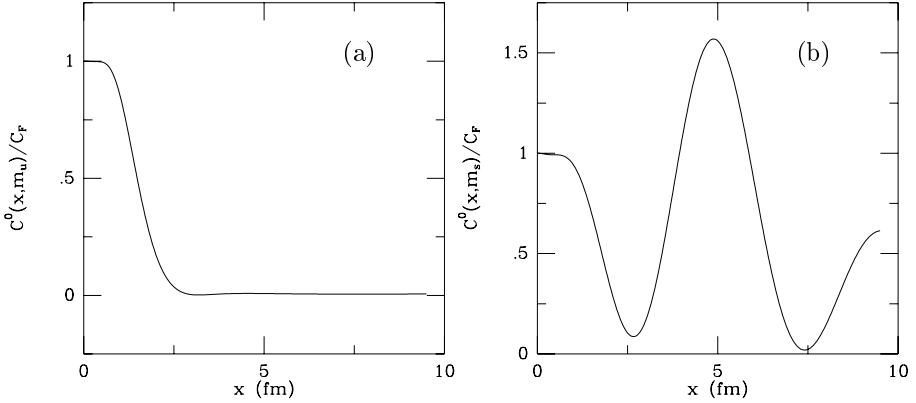


Fig. 9. Large distance behaviour of the connected and normalized correlator $C^0(x, m)$. (a) for up (down) and (b) for strange quarks.

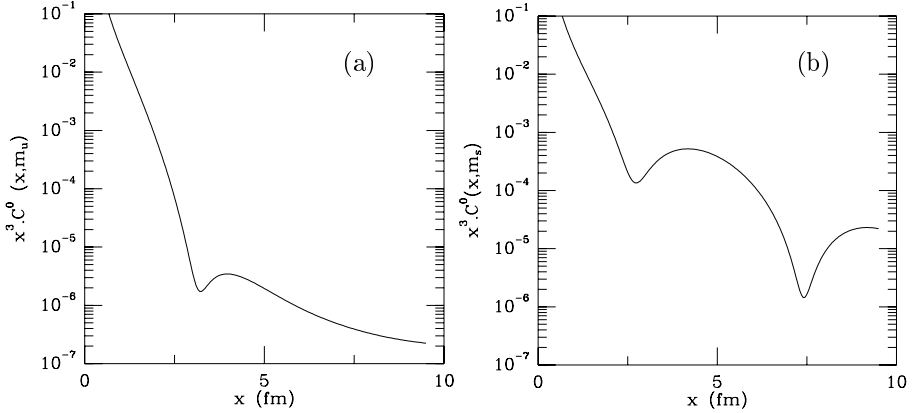


Fig. 10. Large distance behaviour of the connected correlator times x^3 . (a) for up (down) quark, and (b) for strange quark, respectively.

in at about 2.5 fm. From the asymptote, we read a slope of $m_\pi \sim 157$ and 215 MeV, respectively. The agreement of the slopes with the GOR result provides consistency checks on the various Fourier transforms performed. We stress that to read the masses through slopes requires a proper identification of the preexponent power (here $x^{-3/2}$). A raw plot of the total correlator *versus* x does not show any scaling up to 10 fm!

A similar analysis for the kaon channel is shown in Fig. 12, where only the rescaled and unconnected part $C^1(x)$ is shown. The connected part oscillates at distances of the order of 2.5 fm and larger, as shown in Fig. 9(b), for two strange quarks. In contrast to the pion channel, the ratio of the connected

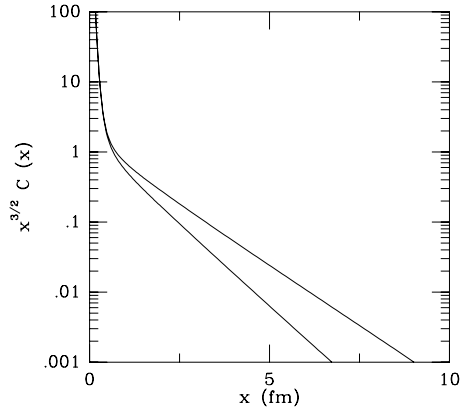


Fig. 11. In the pion channel, the total correlator times $x^{3/2}$ versus x (fm) is plotted for $m_u=5$ MeV (upper curve) and $m_u=10$ MeV (lower curve), respectively.

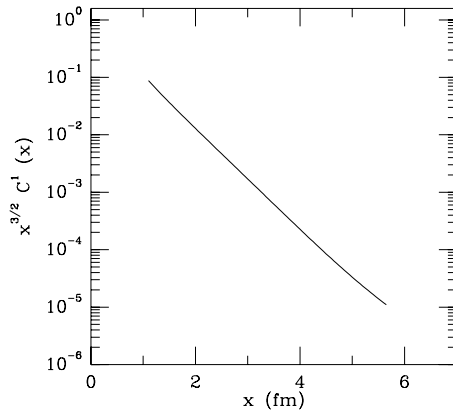


Fig. 12. In the kaon channel, the connected correlator times $x^{3/2}$ versus x (fm) is plotted for $m_s=140$ MeV.

to unconnected parts in this case is about 5:1. The linear fall off in Fig. 12 sets in between 2 and 3 fm. From the slope, we read $m_K = 490$ MeV, for $m = 5$ MeV and $m_s = 140$ MeV. We note that all the non-linearities in the strange quark mass cancel out to give a kaon mass that is compatible with the mass obtained by a naive use of the GOR relation, as indicated above.

• η and η'

In the η and η' channels, the situation is a bit more subtle because of mixing and the anomaly. First, let us follow the nonet decomposition used in Appendix D, for the singlet (κ_0) and the octet (κ_8) excitations. The connected part of the correlator in the (00,08,88) channels reads

$$C^0(p) = - \int dk \text{Tr} (\gamma_5 \lambda_\eta S(k_1, m) \gamma_5 \lambda_\eta S(k_2, m)) \tag{48}$$

with λ_η any of the singlet or octet U(3) generator. Specifically,

$$\begin{aligned} C_0^0(x) &= \frac{4}{3} C^0(x, m_u) + \frac{2}{3} C^0(x, m_s), \\ C_8^0(x) &= \frac{2}{3} C^0(x, m_u) + \frac{4}{3} C^0(x, m_s), \\ C_{08}^0(x) &= \frac{2\sqrt{2}}{3} (C^0(x, m_u) - C^0(x, m_s)) \end{aligned} \tag{49}$$

with $C^0(x, m_u)$ and $C^0(x, m_s)$ the correlators of two screened uu and ss quarks, with $m_u = m_d = 10$ MeV and $m_s = 140$ MeV. The behaviour of (49) is shown in Fig. 13 *versus* x . The oscillations seen in all channels beyond 2.5 fm are due to the spurious quark modes.

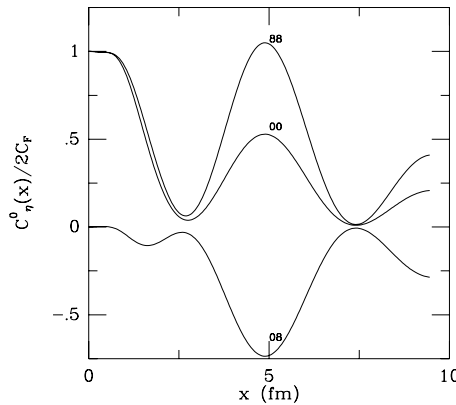


Fig. 13. The connected correlator (normalized to the free and massless correlator) for the η (00,88,08) *versus* x (fm).

The unconnected part of the correlators in the singlet, octet and mixed channels follow from the results of Appendix D. Since the η_0 and η_8 fields are integrated over, we can disentangle them by a unitary rotation of angle θ ($\Delta = \Delta_-(k, m, m)$, $\Delta_s = \Delta_-(k, m_s, m_s)$ and $z = \chi_* N_f / N_c$)

$$\sin 2\theta(p) = \frac{4\sqrt{2}}{3} \frac{\Delta - \Delta_s}{\lambda_+(k) - \lambda_-(k)}, \tag{50}$$

where

$$\lambda_{\pm}(k) = \Delta + \Delta_s + \frac{z}{2} \pm \left(\left(\Delta - \Delta_s + \frac{z}{2} \right)^2 + \frac{2z}{3} (\Delta_s - \Delta) \right)^{1/2}, \quad (51)$$

at the expense of rotating the vertices (sources) as well. The result is

$$C_0^1(p) = 2N_c \left(\frac{(R_0 \cos \theta + R_{08} \sin \theta)^2}{\lambda_+(k)} + \frac{(-R_0 \sin \theta + R_{08} \cos \theta)^2}{\lambda_-(k)} \right), \quad (52)$$

$$C_8^1(p) = 2N_c \left(\frac{(R_{08} \cos \theta + R_8 \sin \theta)^2}{\lambda_+(k)} + \frac{(-R_{08} \sin \theta + R_8 \cos \theta)^2}{\lambda_-(k)} \right), \quad (53)$$

$$C_{08}^1(p) = 2N_c \frac{(R_0 \cos \theta + R_{08} \sin \theta)(R_{08} \cos \theta + R_8 \sin \theta)}{\lambda_+(k)} \\ + 2N_c \frac{(-R_0 \sin \theta + R_{08} \cos \theta)(-R_{08} \sin \theta + R_8 \cos \theta)}{\lambda_-(k)}. \quad (54)$$

The poles in the unconnected parts are just the η and η' masses, since we have rewritten the singlet and octet correlators in the η and η' basis⁵. At low momentum $\theta \sim -13.1^\circ$, which is to be compared with $\theta \sim -11.5^\circ$ in [17]. From the effective action of Appendix D, we conclude that to leading order in the current masses

$$\lambda_{\pm}(k \sim 0) = -\frac{m + m_s}{2N_c} \langle \bar{\psi} \psi \rangle + \frac{z}{2} \\ \pm \left(\left(\frac{m_s - m}{2N_c} \langle \bar{\psi} \psi \rangle + \frac{z}{2} \right)^2 + \frac{2z}{3} \frac{m_s - m}{2N_c} \langle \bar{\psi} \psi \rangle \right)^{1/2}. \quad (55)$$

Then,

$$f^2 m_{\eta'}^2 = 2N_c \lambda_+(k \sim 0) \quad (56)$$

and

$$f^2 m_{\eta}^2 = 2N_c \lambda_-(k \sim 0). \quad (57)$$

The above relations give $m_{\eta'} = 1163$ MeV and $m_{\eta} = 557$ MeV. These values are to be compared with $m_{\eta'} = 1172$ MeV and $m_{\eta} = 527$ MeV for $\langle \bar{\psi} \psi \rangle = (-255 \text{ MeV})^3$ and $f = 91$ MeV as used in Ref. [17]. From (55), (56) and (57) we have

$$f^2 (m_{\eta'}^2 + m_{\eta}^2 - 2m_K^2) = 2N_f \chi_* \quad (58)$$

which is the Veneziano–Witten formula [25, 33].

⁵ Since the diagonalization is momentum dependent, it is not possible to devise a local source that would trigger precisely the η or η' quantum numbers without mixing.

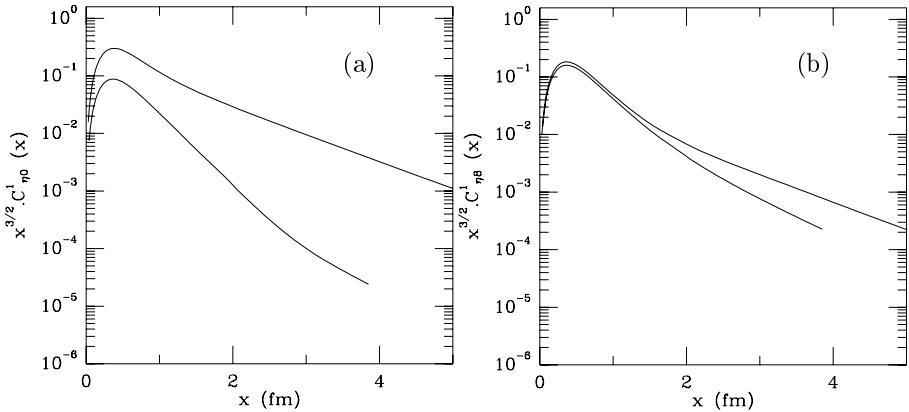


Fig. 14. The unconnected correlator times $x^{3/2}$ for the (00) channel (a) and the (88) channel (b) *versus* x (fm) is plotted with (upper curve) and without (lower curve) a topological susceptibility.

Figs 14(a) and (b) show the behaviour of the rescaled and unconnected parts of the correlators *versus* x . At about 3 fm, the asymptotic slopes set in. The large distance behaviour being dictated by the smaller pole, we obtain a slope of 220 MeV (essentially the pion mass) when the term $\chi_* N_f / N_c$ is switched off, and a slope of 480 MeV (essentially the η mass) when it is not. The contribution due to the large η' mass dies off too rapidly, as seen from the asymptotic behavior. In this sense, it is very hard to measure the η' characteristics from an x -space analysis of the correlation functions. The x -space analysis of the topological susceptibilities offers a better probe [21], although on the lattice there may be subtleties related to the definition of gluonic sources. Finally, we note that in the presence of the connected parts of the correlator, no asymptote sets in within 5 fm due again to the spurious oscillations discussed above.

We note that since $\chi_* = n \sim N_c$, the instanton-induced shift in the η' mass $2\chi_* N_f / f^2 \sim N_c^0$, at variance with Witten's argument [25]. This is not totally surprising, if we recall that the original instanton gauge-configuration $A \sim 1/g \sim \sqrt{N_c}$. Also for $n \sim N_c$, we have a fixed compressibility $\sigma_* \sim N_c^0$. However, when the density n grows, the instanton and antiinstanton system is no longer dilute, and one would a priori expect a phase change [23], whence a breakdown of the conventional large N_c arguments. The academic case of $n \sim N_c^0$ yields zero compressibility, with the quantum fluctuations dwarfing the instanton effects.

5.3. Scalars

In Fig. 15 we plot the (normalized) connected $C^0(x)$ and unconnected $C^1(x)$ parts of the correlator in short and long dashed lines respectively. The solid line represents the sum of these two. As seen from Fig. 3(d) the contribution from the first three diagrams is non vanishing in the scalar channel. If we were to repeat the calculation leading to the unconnected part of the correlator in x -space we would obtain the additional term

$$N_c \int \text{Tr} S(k, m) \left(N_c \int \text{Tr} S(k, m) - 2 \int \frac{M_k}{\Delta_+(k-l)} \text{Tr} C^2(k, m) (B(l, m) \not{l} + iA(l, m)) \right). \quad (59)$$

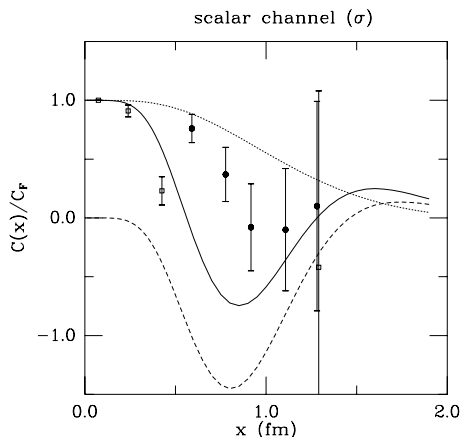


Fig. 15. The scalar connected and unconnected sigma meson-correlator (normalized to the free and massless correlator) *versus* x (fm) for $m_u = m_d = 10$ MeV are respectively plotted in short dashed and long dashed lines. The solid line represents their sum. The squares are the results obtained in [36] using 128 instantons and 128 antiinstantons in a periodic box. The circles are the results obtained in [4] from cooled lattice gauge calculations.

If we recall the definition for the unconnected correlator we expect this additional term to be amenable to the square of the condensate $\langle \overline{\psi\psi} \rangle$. The decay constant and the sigma meson mass follow from the last diagram of Fig. 3(d). They can be evaluated through the use of a similar expansion of Δ_- to Δ_+ . Specifically

$$f^2 = 4N_c \int \frac{d^4k}{(2\pi)^4} \frac{M_k^2}{4\mathcal{D}^2} \left(\left(\frac{M_k'}{k} + M_k'' \right) \left(1 - \frac{2M_k^2}{\mathcal{D}} \right) - \frac{M_k}{2\mathcal{D}} \left(1 + \frac{M_k'^2}{4} - \frac{k^2}{2\mathcal{D}} \left(1 + \frac{M_k M_k'}{k} \right)^2 \right) \right) \quad (60)$$

and the scalar mass M_+ is given by

$$\frac{f^2}{4N_c} M_+^2 = 2m \left(\frac{n}{2N_c} \lambda(m) - \int \frac{d^4k}{(2\pi)^4} \frac{M_k}{\mathcal{D}} \right) \left(1 - \frac{8M_k^2 k^2}{\mathcal{D}} \right) + \int \frac{1}{8\pi^2} \frac{4M_k K^2}{\mathcal{D}^2}, \quad (61)$$

where $\mathcal{D} = k^2 + M_k^2$. Numerically, we obtain $m_\sigma = 640$ MeV and $f = 109$ MeV. The scalar mass is about twice the constituent mass of $2 \times 310 = 620$ MeV. This is generic of all bosonized interactions at the mean-field level (*e.g.* Nambu–Jona-Lasinio model). The nearness of the quark–antiquark threshold is expected to yield a large width for the scalar–isoscalar.

5.4. Vectors

- ρ , K^* and ϕ

To leading order in the instanton density, the vector correlation functions for both the ρ and ϕ do not acquire any unconnected part. (The vector correlation functions are just the correlation functions of two screened quarks.) This is expected, since the instanton–antiinstanton interaction acts primarily in the spin–isospin zero channel. Figs 16 and 17 show respectively, the behaviour of the ρ -, and ϕ -correlators *versus* x up to 2 fm, for a light quark mass of 5 MeV and a strange quark mass of 140 MeV. The squares in these figures correspond to the instanton simulations, while the filled circles in Fig. 15 correspond to the cooled and quenched lattice simulations. The failure to produce correlations in the vector channel, while obvious in the p -space analysis, is implausible from the x -space analysis. In general, simple spectral guesses as used in the instanton simulations or lattice calculations for an x -space analysis within 1 to 2 fms may be misleading. They cannot differentiate between cuts and poles within 1.5 fm. At these distances it is difficult to reliably differentiate between poles and cuts (the pion-channel being an exception). A resolution of the two requires a careful analysis of the preexponents and the asymptotics, as we have discussed.

In the case of the K^* , it is clear that a contribution due to the mixing between the up (down) and strange sectors occurs in the unconnected part

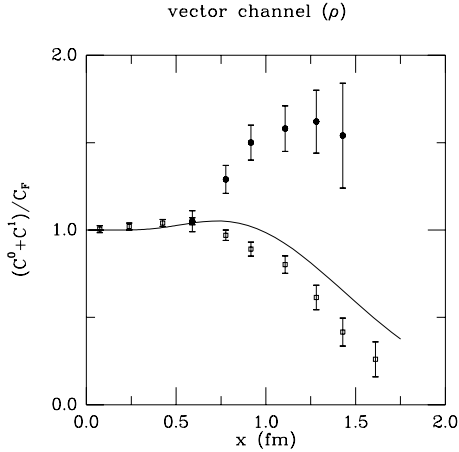


Fig. 16. The total correlator (normalized to the free and massless correlator) in the ρ meson channel *versus* x (fm), for $m_u = m_d = 10$ MeV. The squares are the results of [36] using 128 instantons and 128 antiinstantons in a periodic box.

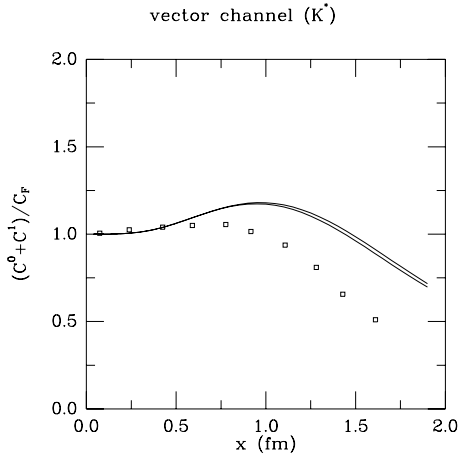


Fig. 17. The total correlator (normalized to the free and massless correlator) in the ϕ meson channel *versus* x (fm), for $m_u = m_d = 10$ MeV. The squares are the results of [36] using 128 instantons and 128 antiinstantons in a periodic box.

of the correlator. This is evident from Appendix E, where we see that the coupling of the ρ and ϕ to the quarks vanishes identically, whereas in the case of the K^* a contribution in $\mathcal{O}(m_s - m_u)$ arises. The possibility of the unconnected part of the K^* -correlator being contaminated by the excitations of its scalar partner (in flavor space) π_s^K is allowed. Having said this we display in Fig. 18 the behaviour of the K^* -correlator *versus* x up to

2 fm, for a light quark mass of both 5 MeV (upper curve) and 10 MeV (lower curve), and a strange quark mass of 140 MeV. Again, the squares in this figure correspond to the instanton simulation.

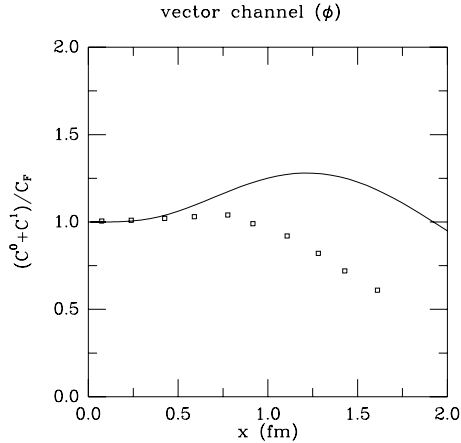


Fig. 18. The total correlator (normalized to the free and massless correlator) in the K^* meson channel *versus* x (fm), for $m_u = m_d = 5$ MeV (upper curve) and $m_u = m_d = 10$ MeV (lower curve). The squares are the results of [36] using 128 instantons and 128 antiinstantons in a periodic box.

- A_1 and K_1 .

Similar conclusions apply to the axial-vector correlators, although the latter are contaminated by pion and kaon excitations through their longitudinal parts. Generically, the nonstrange axial-vector correlator can be decomposed along the transverse and longitudinal directions that consist of the A_1 and π , respectively:

$$C_{\mu\nu}(p) = (\delta_{\mu\nu} - \hat{p}_\mu \hat{p}_\nu) C^T(p) + \hat{p}_\mu \hat{p}_\nu C^L(p). \quad (62)$$

From the p -space analysis, each contribution is well separated. C^T contains solely a cut, while C^L displays only a pole. Similar remarks apply to the strange axial-vector correlator K_1 . Figs 19 and 20 show the behaviour of the combination $3C^T + C^L$ *versus* x in the A_1 and K_1 channel, respectively. The squares refer to the results of simulations using instantons.

Since the longitudinal pole reflects on the pion pole, consistency with the pseudoscalar correlators requires that the pion properties (mass and decay constant) should be the same. The explicit form of the longitudinal part of

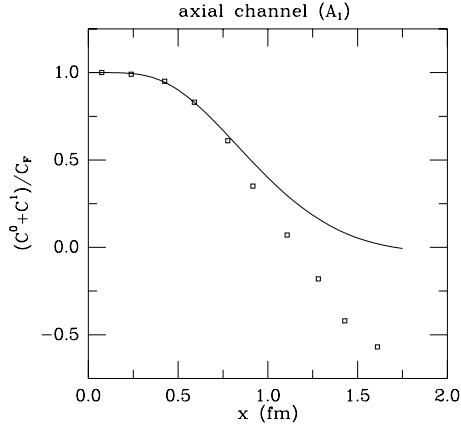


Fig. 19. The total correlator (normalized to the free and massless correlator) in the A_1 meson channel *versus* x (fm), for $m_u = m_d = 10$ MeV. The squares are the results of [36] using 128 instantons and 128 antiinstantons in a periodic box.

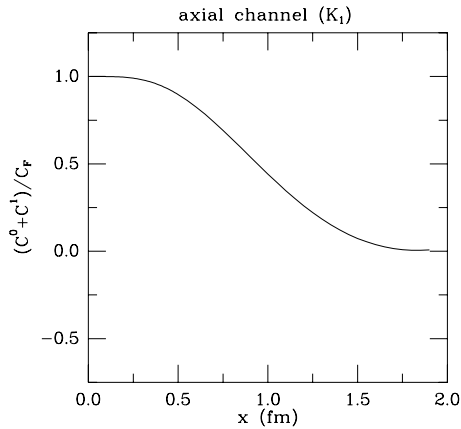


Fig. 20. The total correlator (normalized to the free and massless correlator) for the K_1 meson channel *versus* x (fm) for $m_u = m_d = 10$ MeV.

the axial correlator reads

$$C_{\mu\nu}^L(p) = \hat{p}_\mu \hat{p}_\nu 2N_c \frac{\left(R_{\gamma_5 \gamma_\mu}^+(p)\right)^2}{\Delta_-(p)}, \quad (63)$$

where at zero momentum

$$R_{\gamma_5 \gamma_\mu}^+(p=0) = 2 \int \frac{d^4 k}{(2\pi)^4} \frac{M_k^2 - k M_k M'_k / 2}{(k^2 + M_k^2)^2} \quad (64)$$

which is just $f_\pi^2/2N_c$. Numerically, we obtain from the axial-correlator $f_\pi = 76$ MeV, which is about 10 % off from the value of $f_\pi = 88$ MeV extracted from the pseudoscalar-correlator. This point illustrates some of the systematic uncertainties introduced by the use of undistorted scattering states for the nonzero mode states around a single instanton or antiinstanton [13].

6. Baryon correlators

In the large N_c limit, a baryon is made out of N_c quarks, and is believed to be a soliton [25]. In our case, we will think of a nucleon as made of $N_c = 3 \gg 1$ quarks. To leading order in $1/N_c$, the nucleon is just three free streaming constituent quarks. In contrast to the meson case, the induced instanton (or gluon interaction) interaction between diquarks is subleading in $1/N_c$. We note that the soliton case in this model was considered in [23].

Generically, the baryonic correlators will be defined to be

$$R(x) = i \langle T^* J_B(x) J_B(0) \rangle, \quad (65)$$

where we use for the nucleon and delta currents

$$\begin{aligned} J^N(x) &= \varepsilon_{abc} \left(u^a(x) C \gamma_\mu u^b(x) \right) \gamma^\mu \gamma_5 d^c(x), \\ J_\mu^\Delta(x) &= \varepsilon_{abc} \left(u^a(x) C \gamma_\mu u^b(x) \right) u^c(x), \end{aligned} \quad (66)$$

respectively. Using Wick's theorem, we can reduce the nucleon and delta correlators into (Minkowski)

$$\begin{aligned} R^N(x) &= 2\varepsilon_{abc}\varepsilon_{a'b'c'} \gamma^\mu \gamma_5 S^{cc'}(x) \gamma^\nu \gamma_5 \text{Tr} \left(\gamma_\mu S^{bb'}(x) \gamma_\nu S^{aa'}(-x) \right), \\ R^\Delta(x) &= 3\varepsilon_{abc}\varepsilon_{a'b'c'} S^{cc'}(x) \text{Tr} \left(\gamma_\mu S^{bb'}(x) \gamma^\nu S^{aa'}(-x) \right). \end{aligned} \quad (67)$$

In the free case, (67) reduces to

$$i \frac{24 \not{x}}{\pi^6 x^{10}} \quad \text{and} \quad -i \frac{18 \not{x}}{\pi^6 x^{10}}, \quad (68)$$

respectively.

Fig. 21 shows the behaviour of three constituent quarks *versus* x . The two solid lines are for 5 and 10 MeV, respectively, the open circles are the results of instanton simulations and the full circles are those of quenched and cooled lattice simulations. Clearly, both simulations show attraction in the nucleon channel, which is very likely due to the fact that in the instanton model, the instanton induced interaction in a spin-zero isospin-zero diquark

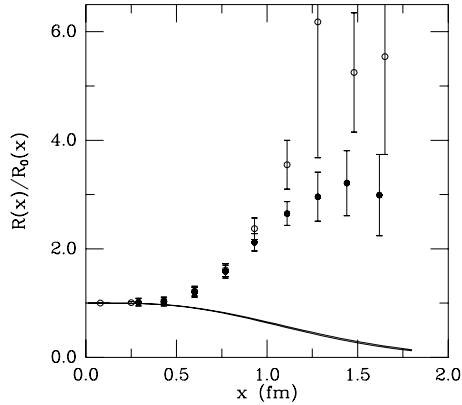


Fig. 21. The total correlator (normalized to the free and massless correlator) in the nucleon channel *versus* x (fm) is plotted for $m_u = m_d = 5$ MeV (upper curve) and for $m_u = m_d = 10$ MeV (lower curve), respectively. The squares are the results obtained in [36] using 128 instantons and 128 antiinstantons in a periodic box. The circles are the results obtained in [4] from cooled lattice gauge calculations.

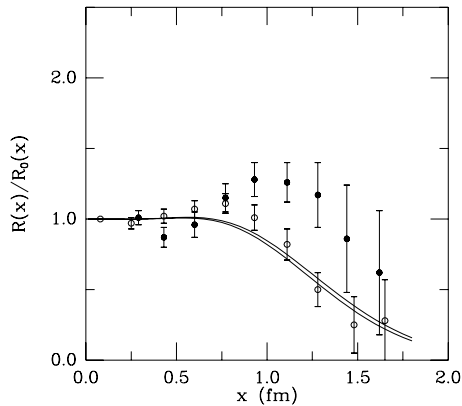


Fig. 22. The total correlator (normalized to the free and massless correlator) in the Δ channel *versus* x (fm) is plotted for $m_u = m_d = 5$ MeV (upper curve) and for $m_u = m_d = 10$ MeV (lower curve). The squares are the results obtained in [36] using 128 instantons and 128 antiinstantons in a periodic box. The circles are the results obtained in [4] from cooled lattice gauge calculations.

configuration $(qq)_{I=0}^{J=0}$ is attractive. This follows from the large attraction already observed in the spin-zero isospin-zero quark–antiquark configuration $(\bar{q}q)_{I=0}^{J=0}$ by crossing. This attraction is, however, an order of magnitude smaller than the attraction in the pion channel. Whether these interactions can result in a pole remains an open question and requires a more detailed

analysis. Indeed, the screened quarks amount to a mass of about 940 MeV, which is close to the empirical value of the nucleon mass.

Fig. 22 shows the results in the delta channel. From this, we conclude that the present simulations cannot distinguish between a cut and a pole in this channel. In fact, it is very unlikely that a dilute instanton gas can yield binding in decuplet channels, since the instanton induced interaction is usually non-existent in these channels.

7. Gluonic correlators

The present construction allows for a convenient analysis of correlation functions involving $F \cdot F$ and $F \cdot \tilde{F}$ reflecting on the scalar and pseudoscalar glueballs in the model [17,21]. In the quenched approximation, these correlators are ultralocal and given by our choice of the measure (5). Through the identification

$$\frac{1}{32\pi^2} F \cdot F(x) = (n^+ + n^-)(x) \quad (69)$$

the scalar gluon correlator reads

$$\begin{aligned} \mathcal{C}_{FF}(x-y) &= \left\langle T^* \frac{1}{32\pi^2} F^2(x) \frac{1}{32\pi^2} F^2(y) \right\rangle_{\text{conn.}, N_f=0} \\ &= \left\langle T^* \left((n^+ + n^-)(x) - n \right) \left((n^+ + n^-)(y) - n \right) \right\rangle_{N_f=0} \\ &= \sigma_*^2 \delta^4(x-y). \end{aligned} \quad (70)$$

Also, through the identification

$$\frac{1}{32\pi^2} F \cdot \tilde{F}(x) = (n^+ - n^-)(x) \quad (71)$$

the pseudoscalar gluon correlator reads

$$\begin{aligned} \mathcal{C}_{F\tilde{F}}(x-y) &= \left\langle T^* \frac{1}{32\pi^2} F\tilde{F}(x) \frac{1}{32\pi^2} F\tilde{F}(y) \right\rangle_{N_f=0} \\ &= \langle T^* (n^+ - n^-)(x) (n^+ - n^-)(y) \rangle_{N_f=0} \\ &= \chi_* \delta^4(x-y). \end{aligned} \quad (72)$$

In (2), the glueballs in the quenched approximation carry infinite mass and zero size. They act as heavy sources.

In the presence of quarks, the glueball sources mix. The mixing is of order $1/N_c$. In the scalar channel,

$$\begin{aligned} \mathcal{C}_{FF}(x-y) &= \left\langle T^* \left((n^+ + n^-)(x) - n \right) \left((n^+ + n^-)(y) - n \right) \right\rangle \\ &= \sigma_*^2 \left(\delta^4(x-y) + 2N_f \sigma_*^2 \langle T^* \pi_0(x) \pi_0(y) \rangle \right), \end{aligned} \quad (73)$$

where the unconnected correlator in the λ_0 scalar channel is

$$\langle \pi_0(x) \pi_0(y) \rangle = \frac{1}{2N_c} \int dk e^{ik(x-y)} \left(\frac{2/3}{2\Delta_+(k, m, m)} + \frac{1/3}{2\Delta_+(k, m_s, m_s)} \right). \quad (74)$$

The large separation behaviour of the above result follows from Section 5 with the pole $m_0 = 640$ MeV as the mass of the scalar-isoscalar. Because of the mixing, the fall-off is dictated by the scalar-isoscalar masses. Fig. 23 shows the plot of the scalar correlator $\mathcal{C}_{FF}(x)$ (minus the ultralocal term). From (73) and (74), the compressibility takes the form

$$\sigma^2 = \frac{1}{V_4} \left\langle \left(\int d^4z (n_+ + n_- - n)(z) \right)^2 \right\rangle \simeq \frac{4n}{b}, \quad (75)$$

where b is given by

$$b = \frac{11N_c}{3} - \frac{2N_f}{3} \alpha_+ \quad (76)$$

with

$$\alpha_+ = \frac{n}{N_c} \sum_f \frac{1}{\Delta_+(k=0, m_f, m_f)}. \quad (77)$$

Numerically we find $\alpha_+ = 1.22$, which is to be compared with $\alpha_+ = 1$ in the QCD trace anomaly. This is only suggestive, however, since the two calculations are totally different in spirit. Ours is classical, while in QCD it is quantum. In a similar way, we have in the pseudoscalar channel

$$\begin{aligned} \mathcal{C}_{F\tilde{F}}(x-y) &= \langle T^* (n^+ - n^-)(x) (n^+ - n^-)(y) \rangle \\ &= \chi_* \left(\delta^4(x-y) - 2N_f \chi_* \langle T^* \eta_0(x) \eta_0(y) \rangle \right), \end{aligned} \quad (78)$$

where the unconnected correlator in the λ_0 pseudoscalar channel is

$$\langle \eta_0(x) \eta_0(y) \rangle = \frac{1}{2N_c} \int dk e^{ik(x-y)} \left(\frac{\cos^2 \theta(k)}{\lambda_+(k)} + \frac{\sin^2 \theta(k)}{\lambda_-(k)} \right) \quad (79)$$

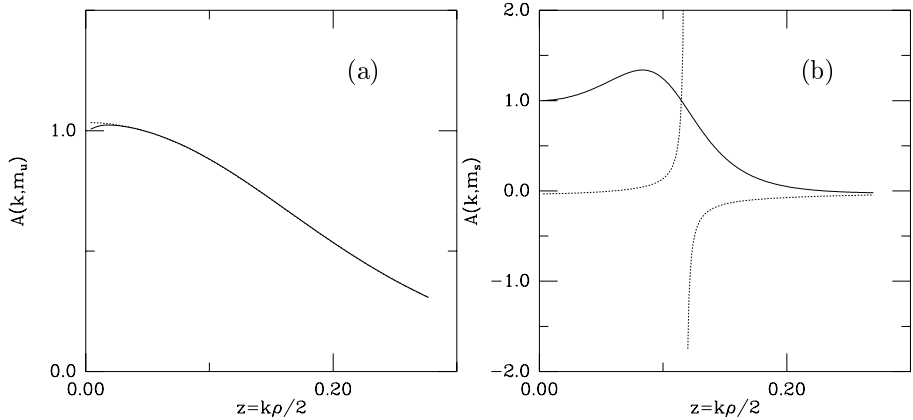


Fig. 23. The coefficient $A(k, m)$ versus $z = k\rho/2$ for up (a) and for strange (b) quarks. The solid line is the unexpanded result and the dotted line is the expanded result.

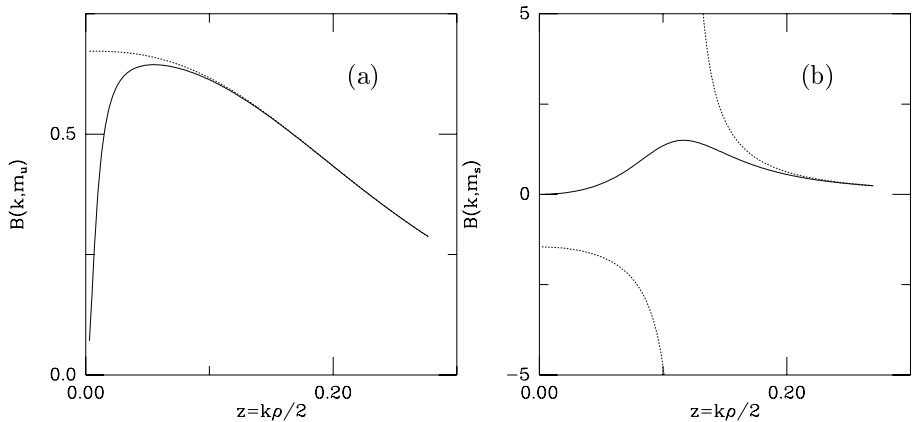


Fig. 24. The coefficient $B(k, m)$ versus $z = k\rho/2$ for up (a) and for strange (b) quarks. The solid line is the unexpanded result and the dotted line is the expanded result.

The rotation angle $\theta(k)$ along with λ_{\pm} are defined in (50) and (51), respectively. The fluctuations in the pseudoscalar gluonic source fall off with a rate that is given by the lightest mass (the η in our case) $m_{\eta} = 557 \text{ MeV}$. Fig. 26(b) shows the plot of the scalar correlator $\mathcal{C}_{F\tilde{F}}(x)$ (minus the ultralocal term). Let us now evaluate $\mathcal{C}_{F\tilde{F}}(x - y)$ using the pseudoscalar field decomposition, in which the quadratic part of the action is diagonal. We

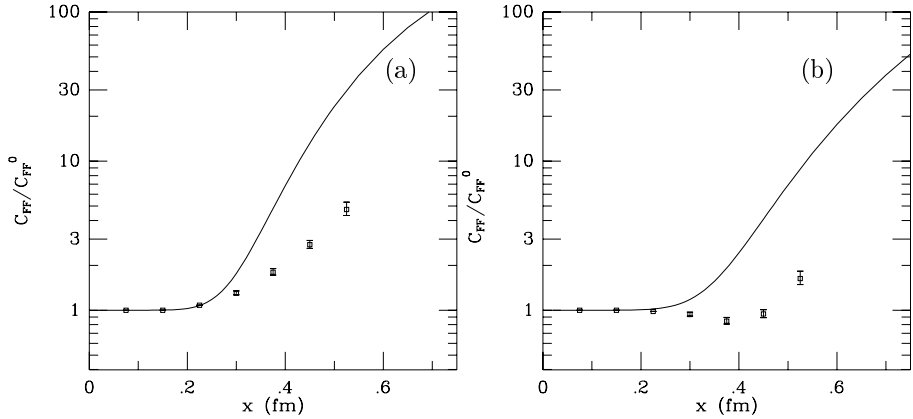


Fig. 25. The scalar (pseudoscalar) gluonic correlator is plotted in this figure. The points are results from simulations in [34].

obtain

$$\mathcal{C}_{F\bar{F}}(x-y) = \int dk e^{ik(x-y)} \left(\frac{1}{\chi_*} + \frac{1}{2N_c} \sum_{i=1}^{N_f} \frac{1}{\Delta_-(k, m_i, m_i)} \right)^{-1}. \quad (80)$$

One should not be alarmed by the two different expressions for the pseudoscalar gluonic correlators (78) and (80). Using the two relations (denoting $\Delta = \Delta_-(k, m, m)$ and $\Delta_s = \Delta_-(k, m_s, m_s)$)

$$\lambda_+(k)\lambda_-(k) = 4\Delta\Delta_s + \frac{2}{3} \frac{\chi_* N_f}{N_c} (\Delta + 2\Delta_s) \quad (81)$$

and

$$\lambda_+(k) \sin^2 \theta(k) + \lambda_-(k) \cos^2 \theta(k) = \frac{2}{3} (\Delta + 2\Delta_s) \quad (82)$$

we can easily rewrite (80) to (78). The mixing causes the topological susceptibility to decrease. From (80) we have

$$\chi = \frac{1}{V_4} \left\langle \left(\int d^4z (n_+ - n_-)(z) \right)^2 \right\rangle = \frac{\chi_*}{1 - \sum_{i=1}^{N_f} \frac{\chi_*}{m_i \langle \bar{\psi}\psi \rangle}} \quad (83)$$

and vanishes for any quark mass going to zero. The topological charge is totally screened in the chiral limit.

8. Nucleon form factor

All hadrons are characterized by various form factors, each of which carry information on the various charge and current distributions. In this part, we show how various nucleon form factors can be analyzed in $1/N_c$, thinking of $N_c = 3 \gg 1$. In this Section, we will distinguish between purely gluonic form factors $\mathbf{G}(x) \sim F^2(x), F\tilde{F}(x), \sigma_{\mu\nu}F^\mu F^\nu, \dots$ and fermionic form factors $\mathbf{F}(x) = \psi^\dagger \mathbf{\Lambda} \psi$, where $\mathbf{\Lambda} = \gamma \otimes T$ is a spin-flavor matrix. Mixed form factors $\mathbf{M}(x) = \psi^\dagger \sigma_{\mu\nu} F_{\mu\nu} \psi, \dots$ can be obtained in a similar way, although they will not be discussed here.

- Gluonic form factor of a constituent quark

Since the model lacks confinement, the nucleon form factor receives contribution from the unconfined constituent quark states. This is represented in Figs 26(a) and (b) as P^\pm insertions. To leading order in $1/N_c$, these contributions are either direct as shown in Fig. 26(a), or meson mediated (Figs 26(c) and (d)). The constituent quark gluonic form factor is defined (when $x \rightarrow \infty$) as

$$\mathbf{F}_G(k^2) \left\langle T^* \psi \left(\frac{x}{2} \right) \psi^\dagger \left(-\frac{x}{2} \right) \right\rangle = \left\langle T^* \psi \left(\frac{x}{2} \right) \mathbf{G}(k) \psi^\dagger \left(-\frac{x}{2} \right) \right\rangle_{\text{con.}} \quad (84)$$

with

$$\mathbf{G}(k) = \int dy e^{ik \cdot y} \mathbf{G}(y). \quad (85)$$

Throughout, we will think of \mathbf{F}_G as matrix valued (here in spin space), so that various components of the form factor can be extracted by proper

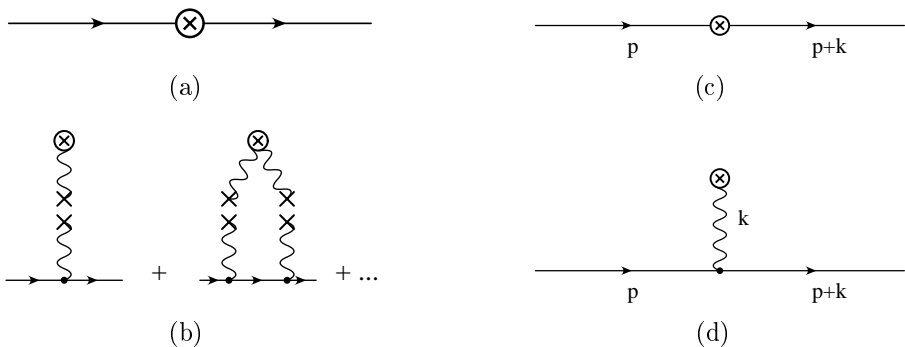


Fig. 26. In (a) and (b), we display the insertion mechanism involved in evaluating the gluonic form factor of a constituent quark. Figures (c) and (d) show the mixing that enters in the connected part.

tracing. To leading order in $1/N_c$, the form can be readily evaluated using the bosonization results developed in Appendices C and D. The result is ($x \rightarrow \infty$)

$$\mathbf{F}_{FF}(k^2)S(x, m) = i \int dp e^{ip \cdot x} \sqrt{M_{p_-} M_{p_+}} C(p_-) 32\pi^2 \langle \pi_s(-k) \sigma(k) \rangle C(p_+) \quad (86)$$

for a scalar gluon insertion, and

$$\begin{aligned} \mathbf{F}_{F\tilde{F}}(k^2) S(x, m) = \\ i \int dp e^{ip \cdot x} \sqrt{M_{p_-} M_{p_+}} C(p_-) i 32\pi^2 \gamma_5 \langle \pi_{ps}(-k) \chi(k) \rangle C(p_+) \end{aligned} \quad (87)$$

for a pseudoscalar gluon insertion. Here $p_{\pm} = p \pm k/2$. The mixed spin-gluon matrix element can be discussed using similar arguments. The expectations in (86)–(87) involve a Gaussian integral over the effective bosonic fields, with quadratic actions as discussed in Appendix C. After integration, the results are ($x \rightarrow \infty$)

$$\begin{aligned} \mathbf{F}_{FF}(k^2) S(x, m) = +i \int dp e^{ip \cdot x} \sqrt{M_{p_-} M_{p_+}} C(p_-) C(p_+) \\ \times \frac{32\pi^2}{2N_c \Delta_+(k, m, m)} \left(\frac{n}{n_* \sigma_*^2} + \frac{1}{2N_c} \sum_f \frac{1}{\Delta_+(k, m_f, m_f)} \right)^{-1} \end{aligned} \quad (88)$$

and

$$\begin{aligned} \mathbf{F}_{F\tilde{F}}(k^2) S(x, m) = +i \int dp e^{ip \cdot x} \sqrt{M_{p_-} M_{p_+}} C(p_-) \gamma_5 C(p_+) \\ \times \frac{32\pi^2}{2N_c \Delta_-(k, m, m)} \left(\frac{1}{\chi_*} + \frac{1}{2N_c} \sum_f \frac{1}{\Delta_-(k, m_f, m_f)} \right)^{-1}. \end{aligned} \quad (89)$$

From our numerical analysis of Section 3, the constituent quark propagator $S(x, m)$ shows a rough scaling in the window $0 < x < 2.5$ fm, with $M_0 \sim 300 - 400$ MeV, but then oscillates for $x > 2.5$ fm, due to non-analyticities. In the window $0 - 2.5$ fm,

$$S(x, m) \sim \frac{iM_0^2}{4\pi^2 x} \sqrt{\frac{\pi}{2M_0 x}} e^{-M_0 x} (\hat{x} + 1). \quad (90)$$

It would be interesting to see how the present form factors (88)–(89) with (90) compare with simulations in the range $0 < x < 2.5$ fm. This is only

indicative, since the channel is contaminated by spurious oscillations for $x > 2.5$ fm.

The large x separation provides for a way to select the constituent quark on its “mass-shell”⁶, hence the analogy with the Minkowski definition of the form factor. We can also define a totally “off-shell” form factor by considering (88)–(89) for finite x and integrating x over V_4 . In this way, one obtains off-mass shell form factors with zero-momentum constituent quarks. For $k = 0$, the results are

$$\mathbf{F}_{FF}^*(0) = \frac{1}{2N_c \Delta_-(0, m, m)} \left(\frac{n}{n_* \sigma_*^2} + \frac{1}{2N_c} \sum_f \frac{1}{\Delta_+(0, m_f, m_f)} \right)^{-1} \quad (91)$$

and

$$\mathbf{F}_{F\tilde{F}}^*(0) = \frac{1}{2N_c \Delta_-(0, m, m)} \left(\frac{1}{\chi_*} + \frac{1}{2N_c} \sum_f \frac{1}{\Delta_-(0, m_f, m_f)} \right)^{-1}. \quad (92)$$

To leading order in $1/N_c$, the “off-shell” scalar form factor reduces to

$$\mathbf{F}_{FF}^*(0) = \frac{3}{11N_c} \alpha, \quad (93)$$

where $\alpha = 2\alpha_+ \sim 2.45$. We note that (93) differs by almost a factor of 2 from its “on-shell” analogue with $\alpha = 1$, as argued from a QCD low-energy theorem based on the trace anomaly [26, 37]. For the pseudoscalar form factor (92) the result is $\mathbf{F}_{F\tilde{F}}^*(0) = 0.44$, which is to be compared with the gluonic part of the “on-shell” value of the axial-singlet form factor g_A^0 , as determined from the U(1) anomaly (8) in the constituent quark state

$$g_A^0(0) \left\langle T^* \psi^\dagger \left(\frac{x}{2} \right) \gamma_5 \psi \left(-\frac{x}{2} \right) \right\rangle = \left\langle T^* \psi^\dagger \left(\frac{x}{2} \right) \left(\int dz \frac{F\tilde{F}(z)}{32\pi^2} + \frac{i}{N_f} \int dz \text{Tr}_f m \psi^\dagger \gamma_5 \psi(z) \right) \psi \left(-\frac{x}{2} \right) \right\rangle_{\text{conn}}. \quad (94)$$

The mass term in (94) involves the $U_A(1)$ form factor in the constituent quark state. In the last few years, efforts have been made to understand the data from the European Muon Collaboration (EMC) [38–46]. One of its remarkable results has been to yield a small value for the singlet axial coupling constant $g_A^0 = 0.13 \pm 0.24$. The result obtained above “off-mass shell” seems to be close to this value. The approach described here, provides some insights from an instanton vacuum model, to the effective approach discussed

⁶ This is, of course, suggestive in Euclidean space.

by many [38, 43, 46]. In fact, the modified bosonisation scheme discussed in Appendix E, is very close in spirit to these models. A comprehensive discussion of all these issues goes beyond the scope of this work.

• Fermionic form factor of a constituent quark

The fermionic form factors can be analyzed in the same way as the gluonic form factors. The mechanism consisting of P^\pm insertion is shown in Fig. 27. In Fig. 28, we show the leading contributions to the mesonic form factor to order $1/N_c$. Fig. 28(a) counts the bare charge, while Fig. 28(b) involves a typical meson-exchange with non-local form factors. Generically ($x \rightarrow \infty$),

$$\mathbf{F}_A(k^2) \left\langle T^* \psi \left(\frac{x}{2} \right) \psi^\dagger \left(-\frac{x}{2} \right) \right\rangle = \left\langle T^* \psi \left(\frac{x}{2} \right) \psi^\dagger \mathbf{A} \psi(k) \psi^\dagger \left(-\frac{x}{2} \right) \right\rangle_{\text{conn}}. \quad (95)$$

Parametrizing all meson fields by $\pi^A = \gamma^A \pi^A$, where $\gamma^A = (1, \gamma_5) \otimes T$, yields to leading order in $1/N_c$

$$\begin{aligned} \mathbf{F}_A(k^2) S(x, m_f) &= -\int dp dq e^{i(p+k/2) \cdot x} \sqrt{M_p} C(p, m_f) \gamma C(q+k, m_g) \sqrt{M_{q+k}} \Lambda \\ &\times \sqrt{M_q} C(q, m_g) \gamma C(k-p, m_f) \sqrt{M_{k-p}} \langle \pi^{fg}(p-q-k) \pi^{gf}(q+k-p) \rangle \\ &+ \int dp e^{i(p-k/2) \cdot x} \sqrt{M_p} C(p, m_f) \gamma C(p-k, m_g) \sqrt{M_{p-k}} \langle \pi^{fg}(k) \pi^{gf}(-k) \rangle \\ &\times \text{Tr} \left(\Lambda \sqrt{M_q} C(q, m_g) \gamma C(q+k, m_f) \sqrt{M_{q+k}} \right), \end{aligned} \quad (96)$$

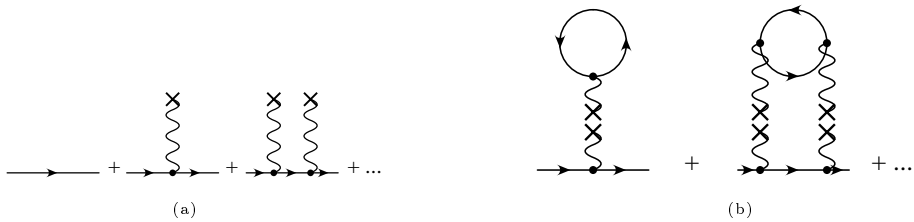


Fig. 27. The insertion mechanism for the fermionic form factor of a constituent quark.

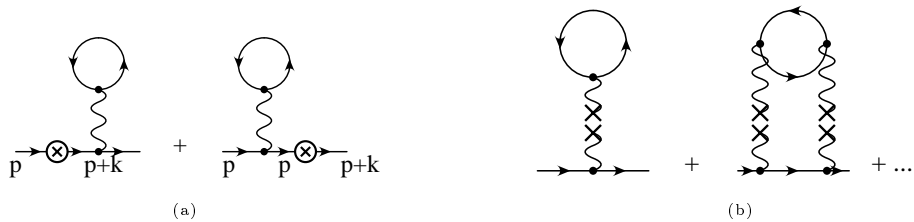


Fig. 28. The leading contributions to the fermionic form factor.

where summation over flavor g is understood and f is the flavor of the quark being probed. γ is 1 (γ_5) for the scalar (pseudoscalar) sector. The first and second terms of (96) are displayed in Fig. 28(a) and 28(b), respectively. The expectation value involves a Gaussian integration over the measure derived in Appendix C and can be evaluated for arbitrary momentum q . In the scalar sector

$$\begin{aligned} \langle \pi_s^{fg}(q) \pi_s^{gf}(-q) \rangle &= \frac{1}{2N_c \Delta_+(q, m_f, m_f)} \left(1 + \frac{1}{2N_c \Delta_+(q, m_f, m_f)} \right) \\ &\times \left(\frac{n}{n_* \sigma_*^2} + \sum_g \frac{1}{2N_c \Delta_+(q, m_g, m_g)} \right)^{-1}. \end{aligned} \quad (97)$$

For the pseudoscalar case, we replace Δ_+ by Δ_- and $n/(n_* \sigma_*^2)$ by $1/\chi$. The case where $\gamma = \gamma_\mu$ (vector form factors) and $\gamma = \sigma_{\mu\nu}$ (tensor form factors) can be analyzed similarly.

It is interesting to note at this stage that most of these form factors may be used to assess the strength of the meson-constituent quark interaction in some constituent quark models, as recently discussed by Glazman and Riska [49]. When couched in the $1/N_c$ framework, the present analysis provides some rationale for their successful phenomenology.

As in the gluonic case, we can investigate the “off-shell” limit of the form factor at $k = 0$. Using (96) for fixed x , integrating numerator and denominator over the entire V_4 , and taking the $k = 0$ limit, yields

$$\begin{aligned} \mathbf{F}_A(0)S(0, m) &= -M_0^2 C(0, m) \gamma \int dq M_q \\ &\times \left(C(q, m) \Lambda C(q, m) \gamma - \text{Tr} (\Lambda C(q, m) \gamma C(q, m)) \right) C(0, m), \end{aligned} \quad (98)$$

where all momenta are taken to be zero. Numerically, the meson-meson expectation value $\langle \pi_s(0) \pi_s(0) \rangle$ in the scalar sector is 0.69 fm^{-4} and 0.92 fm^{-4} , for the up (down) and strange quark, respectively. The same applies for the pseudoscalar sector, where $\langle \pi_{ps}(0) \pi_{ps}(0) \rangle$ is 4.68 fm^{-4} and 6.69 fm^{-4} , for the up (down) and strange quark, respectively. In short, formula (98) along with the numerical values for the meson-meson expectation value, will serve us as a check point when numerically generating the values of $\mathbf{F}_A(k^2)$ using (96).

- Form factors from Ioffe’s currents

If we were to think about the nucleon as made out of three constituent quarks, then the nucleon form factor follows from the additive constituent quark picture. When simulations are performed, however, it is customary

to use Ioffe's currents (66) for the nucleon. This results in some non-trivial combinatorics and folding of the single constituent quark propagators, as we now explain. Let $J_N^\alpha(x)$ be Ioffe's current (66). Then, the nucleon form factor reads ($x \rightarrow \infty$)

$$\mathbf{F}_N(k^2) \left\langle T^* J_N^\alpha \left(\frac{x}{2} \right) \bar{J}_N^\beta \left(-\frac{x}{2} \right) \right\rangle = \left\langle T^* J_N^\alpha \left(\frac{x}{2} \right) \mathbf{O}(k) \bar{J}_N^\beta \left(-\frac{x}{2} \right) \right\rangle, \quad (99)$$

where $\mathbf{O} = \mathbf{G}, \mathbf{F}$, which are short for the gluonic and mesonic insertions discussed above. Typical diagrams for mesonic insertions are displayed in Fig. 29. The term (L.H.S.) multiplying $\mathbf{F}_N(k^2)$ in the left-hand side of (99) can be readily reduced to give (67). The right-hand side (R.H.S.) takes the form

$$\begin{aligned} \text{R.H.S.} = & +6 (\gamma_\mu \gamma_5 \mathcal{O} \mathcal{S}(x; k; m) \gamma_\rho \gamma_5)_{\alpha\beta} \text{Tr}_s (\gamma_\mu \mathcal{S}(x, m) \gamma_\rho \mathcal{S}(-x, m)) \\ & +6 (\gamma_\mu \gamma_5 \mathcal{S}(x, m) \gamma_\rho \gamma_5)_{\alpha\beta} \text{Tr}_s (\gamma_\mu \mathcal{O} \mathcal{S}(x; k; m) \gamma_\rho \mathcal{S}(-x, m)) \\ & +6 (\gamma_\mu \gamma_5 \mathcal{S}(x, m) \gamma_\rho \gamma_5)_{\alpha\beta} \text{Tr}_s (\gamma_\mu \mathcal{S}(x, m) \gamma_\rho \mathcal{O} \mathcal{S}(-x, k, m)), \quad (100) \end{aligned}$$

where $\mathcal{O} \mathcal{S}(x; k; m)$ follows from the right-hand side of (86) and (87) for the gluonic insertions, and, (96) for the mesonic insertions.

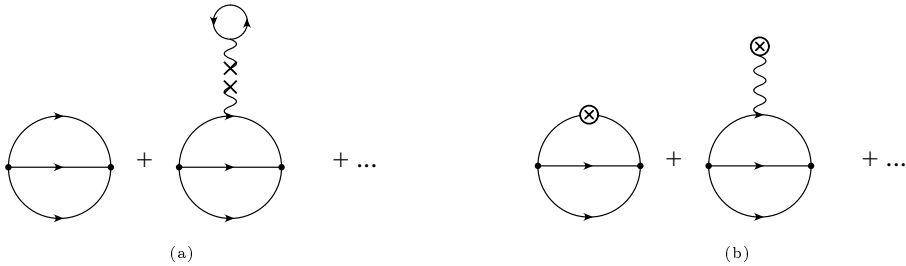


Fig. 29. The form factor in terms of Ioffe's current

It would be interesting to see how (100) compares to actual simulations. As noted above, the actual constituent quark propagator oscillates at distances larger than 2.5 fm. Hence, a true asymptotic form factor may not be reached in this model for the nucleon. In the region $0 < x < 2.5$ fm, the constituent quark propagator seems to be damped following the behaviour described in (90). Using this behaviour, the left-hand side term in (99) reduces to

$$\begin{aligned} \text{L.H.S.} = & \left(\frac{iM_0^2}{4\pi^2 x} \sqrt{\frac{\pi}{2M_0 x}} e^{-M_0 x} \right)^3 \\ & \times 6 (\gamma_\mu \gamma_5 \mathcal{O} \mathcal{S}(\hat{x} + 1) \gamma_\rho \gamma_5)_{\alpha\beta} \text{Tr}_s (\gamma_\mu (\hat{x} + 1) \gamma_\rho (-\hat{x} + 1)) \quad (101) \end{aligned}$$

while the right-hand side reduces to

$$\begin{aligned}
 \text{R.H.S.} &= 6 \left(\frac{iM_0^2}{4\pi^2 x} \sqrt{\frac{\pi}{2M_0 x}} e^{-M_0 x} \right)^2 \\
 &\times \left((\gamma_\mu \gamma_5 \mathcal{O} \mathcal{S}(x; k; m) \gamma_\rho \gamma_5)_{\alpha\beta} \text{Tr}_s \left(\gamma_\mu (\hat{x} + 1) \gamma_\rho (-\hat{x} + 1) \right) \right. \\
 &+ \left(\gamma_\mu \gamma_5 (\hat{x} + 1) \gamma_\rho \gamma_5 \right)_{\alpha\beta} \text{Tr}_s \left(\gamma_\mu \mathcal{O} \mathcal{S}(x; k; m) \gamma_\rho (-\hat{x} + 1) \right) \\
 &\left. + \left(\gamma_\mu \gamma_5 (\hat{x} + 1) \gamma_\rho \gamma_5 \right)_{\alpha\beta} \text{Tr}_s \left(\gamma_\mu (\hat{x} + 1) \gamma_\rho \mathcal{O} \mathcal{S}(-x; k; m) \right) \right). \quad (102)
 \end{aligned}$$

Numerical results for the resulting form factors will be given elsewhere.

9. Discussion

We have analysed the mesonic correlators in a random instanton gas in momentum space using bosonization techniques, and, in coordinate space by performing direct Fourier transforms. Our starting point was a grand-canonical ensemble of instantons and antiinstantons, where the 't Hooft vertices play the role of "fugacities". The momentum space results are in agreement with the original analysis in both the massless [13] and massive cases [19]. Following 't Hooft's suggestion, the resolution of the η' problem follows by assuming that the topological charge is screened [19, 21], with a finite screening length (non-zero topological susceptibility). This effect is leading in $1/N_c$ counting and results in a contribution of order N_c^0 to the η' mass. Without this effect, the η' would be degenerate with the η .

We remark that a non-vanishing topological susceptibility should not be taken for granted [7]. In the present case, it follows directly from the use of instantons and antiinstantons in a singular gauge. A check would be to repeat the analysis using instantons and antiinstantons in a regular (non-singular) gauge, or, carry out cooled lattice simulations with free boundary conditions.

Our x -space translation of the p -space correlators shows that the results of simulations using either a large sample of instantons and antiinstantons in four dimensions, or quenched and cooled lattice gauge configurations, are in agreement with the Fourier transformed analytical calculations within the reported range of (0–1.5) fm. The recent analysis carried out in Ref. [35] for two flavors differs from the bosonized results [19]⁷, hence our analysis.

We have shown that the running quark mass causes the quark propagator to oscillate at large x . The oscillations are larger for larger quark masses

⁷ Eq. (58) in Ref. [35] relies on a resummation of the quark propagator Eq. (57) which is valid only for zero quark mass.

and affect most of the correlation functions at large distances. These effects are spurious and reflect on the lack of confinement in the model. They are easily subtractable in a p -space analysis. They are harder to track down in an x -space formulation. The extent to which these spurious modes impact on the subtracted results is presently unclear.

We have shown that, while the asymptotics of suitably subtracted correlators yield pseudoscalar masses that are accurate to within a few per cent, the non-asymptotic readings could be as inaccurate as 100 %. From our calculations, the subtracted and rescaled correlators show good asymptotics between 2 and 3 fm. The non-rescaled correlators do not show any reasonable asymptotics even up to 10 fm. This point merits further scrutiny in lattice calculations.

The bosonized results show that while it is possible to infer the existence of light pseudoscalars in a dilute instanton gas, they do not seem to support the appearance of bound vectors. We have explicitly shown that the results of simulations are consistent with the presence of just screened quarks in these channels. We have noted that the use of schematic poles and cuts to analyze the x -space correlators in these channels would have implied otherwise. Due to mixing between the octet and singlet pseudoscalars, we have found it difficult to extract the η and η' masses from the x -space analysis. The extraction is straightforward in the p -space analysis.

We have presented a simple analysis of the baryonic correlators in both the nucleon and the delta channels. The attraction seen in the nucleon channel is expected from general arguments. In this channel, however, it appears to be difficult to identify a nucleon mass without going to the asymptotics, since three screened quarks already yield a mass of the order of 940 MeV. This may cause the nucleon to unbind, although soliton-inspired calculations with constituent quarks seem to suggest otherwise [48]. In this respect, it would be interesting to repeat our analysis by including diquark fields. The results of simulations in the delta channel are also consistent with three constituent quarks. A dilute instanton gas does not induce correlations in the decuplet channels.

Using Ioffe's current for the nucleon, we have worked out various gluonic and mesonic form factors "on- and off-mass" shell, to leading order in $1/N_c$. The form factors are sensitive to the the three constituent quark cut. Moreover, the appearance of spurious oscillations in the single constituent quark propagators causes the form factors to be ill-defined for point-to-point separations that are larger than 2.5 fm. In the region $0 < x < 2.5$ fm, some estimations have been made that would be of some interest for future simulations. The analysis of the nucleon form factor presented in this work could also be extended to other mesonic and baryonic channels. It also provides insights in to some recently used constituent quark models [49].

The fluctuations in the number sum and difference of the instantons and antiinstantons relate directly to the scalar and pseudoscalar glueball correlation functions. In the quenched approximation, the glueballs are infinitely heavy and stable. In the unquenched approximation, they mix with their scalar and pseudoscalar counterparts and decay. The mixing and decay are of order $1/N_c$.

The overall agreement between the instanton simulations and the present analysis within 1.5 fm shows that a random set of instantons and antiinstantons that is suitably stabilized in the infrared is well described by gaussian fluctuations over a mean field solution. The mean field solution follows from a simple bosonisation scheme. It also shows that constituent quark models with dynamically generated masses, *e.g.* Nambu–Jona-Lasinio model, are also likely to give similar results provided that chiral symmetry is dynamically broken. In all these models, however, the subtle issue is that of confinement with its impact on large distance asymptotics and form factors.

This work was supported in part by the US Department of Energy under Grant No. DE-FG-88ER40388.

Appendix A

Generating functional

In this Appendix, we provide the necessary details for the derivation of the generating functional (15) discussed in the text. Although these calculations were extensively used in establishing the results of Refs [19], they were never published. We start by evaluating the color averages occurring in the 't Hooft determinants (1) for $N_f = 1$. For convenience, we will use the shorthand notation $d^4k/(2\pi)^4 \rightarrow dk$ and $d^4x \rightarrow dx$ when integrating out. If we denote by

$$\theta^\pm(z) = \left\langle \int dx \psi^\dagger S_0^{-1} \phi^\pm(x-z) \int dy \phi^{\pm\dagger}(y-z) S_0^{-1} \psi(y) \right\rangle_{U\rho} \quad (103)$$

then its Fourier transform reads

$$\theta^\pm(z) = \int dk dl e^{-i(k-l)z} \theta^\pm(k, l) \quad (104)$$

with

$$\theta^\pm(k, l) = \psi_{i,\alpha}^\dagger(k) (\not{k} - im)_{ij} \langle \phi_{j,\alpha}^\pm(k) \phi_{k,\beta}^{\pm\dagger}(l) \rangle_{U\rho} (\not{l} - im)_{kl} \psi_{l,\beta}(l). \quad (105)$$

Averaging over the color group, we obtain [19,20]

$$\theta^\pm(k, l) = \frac{k\phi'(k)l\phi'(l)}{N_c} \psi_{i,\alpha}^\dagger(k) \left(\left(1 - \frac{imk}{k^2} \right) \gamma_5^\mp \left(1 - \frac{iml}{l^2} \right) \right)_{ij} \psi_{j,\alpha}(l), \quad (106)$$

where $\phi'(k)$ is the Fourier transform of the fermion zero mode profile, and is given by

$$\phi'(k) = \pi\rho^2 \frac{\partial}{\partial z} (I_0(z)K_0(z) - I_1(z)K_1(z))_{z=k\rho/2}. \quad (107)$$

With the use of (13), the partition function (2) takes the form

$$\begin{aligned} Z[\eta, \eta^\dagger] &= \int \mathcal{D}\psi^\dagger \mathcal{D}\psi \mathcal{D}P^\pm \mathcal{D}\pi^\pm (-2im)^N e^{-\int \psi^\dagger S_0^{-1} \psi - \psi^\dagger \eta - \eta^\dagger \psi} \\ &\times \exp \frac{n}{2} \int dz \log \left(1 - \frac{1}{2im} \theta^\pm(z) \right) \\ &\times \exp i \int dk dl P^\pm(k, l) (\pi^\pm(k, l) - \theta^\pm(k, l)), \end{aligned} \quad (108)$$

where the integral in the last exponent is performed in both variables k and l of the bilocal auxiliary fields. The field π^\pm is eliminated using the mean field equation

$$-iP^\pm(k, l) = \frac{n}{2} \int dz \frac{1}{1 - \frac{1}{2im} \pi^\pm(z)} \frac{e^{-i(k-l)z}}{2im}. \quad (109)$$

For $N_f > 1$, the auxiliary fields π^\pm and P^\pm are $N_f \times N_f$ valued along with the average θ^\pm (103) entering the 't Hooft determinants (1). As a result, additional traces over flavor indices will be needed. With this in mind, the previous results can be generalized in a straightforward way. For $m = \text{diag}(m_1, \dots, m_{N_f})$, the result is (after absorbing in the measure a term in the size ρ to have a dimensionless argument in the log)

$$\begin{aligned} Z[\eta, \eta^\dagger] &= \int \mathcal{D}\psi^\dagger \mathcal{D}\psi \mathcal{D}P^\pm e^{-\int \psi^\dagger \mathbf{S}^{-1} [P^+, P^-] \psi - \psi^\dagger \eta - \eta^\dagger \psi} \\ &\times e^{-\frac{n}{2} \int dz \text{Tr}_f \log \left(\frac{4}{n\rho} P^+(z) \frac{4}{n\rho} P^-(z) \right)} e^{2 \int dz \text{Tr}_f m(P^+(z) + P^-(z))} \end{aligned} \quad (110)$$

where $\mathbf{S}^{-1} [P^+, P^-]$ is given in the text (17). At the saddle point $P^\pm = P$, and \mathbf{S} is the quark propagator in the external background P such that in momentum space

$$\mathbf{S}(k, l) = \delta^4(k - l) S(k, m) \quad (111)$$

with $S(k, m)$ written down in (21). From (110), the partition function (15) follows after integration over the fermionic fields.

Appendix B

Quark condensate

In this Appendix, we will show that (31) follows from an exact derivation using the standard definition prior to the bosonization procedure. Following the method used in Ref. [19], the partition function (2) can easily be written as (ignoring fluctuations in the density and switching off the sources)

$$Z = \left\langle \int \mathcal{D}\psi^\dagger \mathcal{D}\psi e^{-\int \psi^\dagger S^{-1} \psi} \right\rangle, \tag{112}$$

where in the one flavor case

$$S^{-1} = S_0^{-1} + \frac{1}{2im} S_0^{-1} \phi_I \phi_I^\dagger S_0^{-1}. \tag{113}$$

The (Euclidian) quark condensate follows as

$$\langle \psi^\dagger \psi \rangle = \frac{1}{V_4 Z} \left\langle \int \mathcal{D}\psi^\dagger \mathcal{D}\psi \int \psi^\dagger \psi e^{-\int \psi^\dagger S^{-1} \psi} \right\rangle, \tag{114}$$

where averaging over all pseudoparticles is understood. Specifically,

$$\langle \psi^\dagger \psi \rangle = -\frac{\langle \text{Tr} S(0, m) \det(-S^{-1}) \rangle}{\langle \det(-S^{-1}) \rangle}. \tag{115}$$

Introducing a set of Grassman variables for the pseudoparticle ensemble, the partition function (112) reads (sum over I, J understood)

$$Z = \left\langle \int \mathcal{D}\psi^\dagger \mathcal{D}\psi \mathcal{D}\chi \mathcal{D}\chi^\dagger e^{-\int \psi^\dagger S_0^{-1} \psi} e^{\chi_I^\dagger (T-im)_{IJ} \chi_J} \right\rangle. \tag{116}$$

Here, T is the kinetic part of the overlap matrix [13, 19] and the integration is over fermionic fields ψ, ψ^\dagger and Grassman variables χ_I, χ_I^\dagger , where I is an integer that runs over all the instantons and antiinstantons in the ensemble. Similarly, the condensate

$$\begin{aligned} \langle \psi^\dagger \psi \rangle &= \frac{1}{V_4 Z} \left\langle \int \mathcal{D}\psi^\dagger \mathcal{D}\psi \mathcal{D}\chi \mathcal{D}\chi^\dagger \left(\int \psi^\dagger \psi - \chi_I^\dagger \chi_I \right) \right. \\ &\quad \left. \times e^{-\int \psi^\dagger S_0^{-1} \psi} e^{\chi_I^\dagger (T-im)_{IJ} \chi_J} \right\rangle. \end{aligned} \tag{117}$$

From the two formulas above, it is easy to show that

$$\langle \bar{\psi}\psi \rangle = -i \langle \psi^\dagger\psi \rangle = -\frac{1}{V_4} \frac{\partial \log Z}{\partial m}. \quad (118)$$

We now shift the fermion fields according to $\psi \rightarrow \psi + i\phi_I\chi_I$ and $\psi^\dagger \rightarrow \psi^\dagger + i\chi_I^\dagger\phi_I^\dagger$ (sum over I understood). We then expand χ and χ^\dagger around the respective classical solution of the shifted action. The remaining integral (117) has now a Gaussian form in $\chi^\dagger\chi$ and can be performed. We obtain

$$\begin{aligned} \langle \psi^\dagger\psi \rangle &= \frac{1}{V_4 Z} \left\langle \int \mathcal{D}\psi^\dagger \mathcal{D}\psi (-2im)^N e^{-\int \psi^\dagger S^{-1}\psi} \right. \\ &\quad \times \left. \left(\int \psi^\dagger \left(-1 + S_0 S^{-1} + S^{-1} S_0 + S_0^{-1} \frac{\phi_I \phi_I^\dagger}{2(im)^2} S_0^{-1} \right) \psi + \frac{N}{im} \right) \right\rangle. \end{aligned}$$

Rewriting the pseudoparticle sum in the exponent as a product over I , and noting that only the first two terms in the Taylor expansion contribute, we can easily perform the color group average to yield

$$\begin{aligned} \langle \psi^\dagger\psi \rangle &= \frac{1}{V_4 Z} \int \mathcal{D}\psi^\dagger \mathcal{D}\psi (-2im)^N e^{-\int \psi^\dagger S_0^{-1}\psi} \\ &\quad \times \left(\int \psi^\dagger \psi + \frac{N}{im} - i \frac{\partial}{\partial m} \right) \prod_I \int dz_I \left(1 - \frac{1}{2im} \theta^\pm(z_I) \right), \quad (119) \end{aligned}$$

where $\theta^\pm(z)$ is given in Appendix A. As in [16], we assume a sufficient amount of coarse graining so as to rewrite the product over I with the result

$$\begin{aligned} \langle \psi^\dagger\psi \rangle &= \frac{1}{V_4 Z} \int \mathcal{D}\psi^\dagger \mathcal{D}\psi (-2im)^N e^{-\int \psi^\dagger S_0^{-1}\psi} \\ &\quad \times \left(\int \psi^\dagger \psi + \frac{n}{2im} \int dz \frac{1 - \dot{\theta}^\pm(z)/2i}{1 - \theta^\pm(z)/2im} \right) e^{\frac{n}{2} \int dz \log(1 - \frac{1}{2im} \theta^\pm(z))}, \quad (120) \end{aligned}$$

where the dot on $\theta^\pm(z)$ indicates the derivative with respect to m . The functional integral above can be evaluated exploiting the same bosonisation scheme used for the partition function Z

$$\begin{aligned} \langle \psi^\dagger\psi \rangle &= \frac{1}{V_4 Z} \int \mathcal{D}\psi^\dagger \mathcal{D}\psi \mathcal{D}P^\pm (-2im)^N e^{-\int \psi^\dagger \mathbf{S}^{-1} [P^+, P^-] \psi} \\ &\quad \times e^{-\frac{n}{2} \int dz \log\left(\frac{4m}{n} P^\pm(z)\right)} \\ &\quad \times e^{(-N+2m \int dz P^\pm(z))} \left(\int \psi^\dagger \psi + \int dz \left(\dot{\theta}^\pm(z) - 2i \right) P^\pm(z) \right), \quad (121) \end{aligned}$$

where $\mathbf{S}^{-1}[P^+, P^-]$ is given in the main text (17). At the saddle point

$$\begin{aligned} \langle \psi^\dagger \psi \rangle &= \frac{1}{V_4 Z} \int \mathcal{D}\psi^\dagger \mathcal{D}\psi \left(\frac{n}{2iP} \right)^N e^{-\int \psi^\dagger S^{-1} \psi} e^{-N(-N+4mP)} \\ &\times \left(\int \psi^\dagger (-1 + 2S_0 S^{-1}) \psi - 4iVP \right), \end{aligned} \quad (122)$$

where (aside from rescaling $M_k(m)$) the quark propagator S is written down in momentum space (21). After performing the integral and properly rescaling P , we recover the expression (31) quoted in the main text for the condensate (in the chiral limit). This result is expected, since to leading order in $1/N_c$, the determinants in (115) cancel out, after factorization (quenched approximation).

Appendix C

Gaussian approximation

In what follows, we give details leading to the Gaussian approximation in the partition function. We can repeat the steps performed in Appendix A with the constraint $n_+ = n_- = n/2$ now relaxed and the parametrization

$$\begin{aligned} n_\pm(z) &= \frac{n^*}{2} + \frac{\sigma(z) \pm \chi(z)}{2}, \\ P^\pm(z) &= P + \tilde{\pi}^\pm(z). \end{aligned} \quad (123)$$

A few comments are in order. In the equations above, $\sigma(z)$ and $\chi(z)$ respectively represent the scalar and pseudoscalar glueball sources. The field $\tilde{\pi}^\pm$ contains pseudoscalar and scalar excitations and will be discussed further below. Following Appendix A, the auxiliary field π^\pm is eliminated using the mean field equation

$$-iP^\pm(k, l) = \frac{n^*}{2} \int dz \frac{e^{-i(k-l)z}}{2im} \frac{1}{1 - \pi^\pm(z)/2im}. \quad (124)$$

Along with the contribution from the measure $\mu(n_+, n_-)$ (5) the bosonized effective action reads

$$\begin{aligned} S_{\text{eff}} &= -N_c \text{Tr} \log \mathbf{S}^{-1}[P^+, P^-] - 2 \int dz \text{Tr}_f m (P^+(z) + P^-(z)) \\ &+ \int dz n_\pm(z) \text{Tr}_f \log \left(\frac{4P^\pm(z)}{n^* \rho} \right) + \int dz n_\pm(z) \log N_f! + \tilde{S}_G, \end{aligned} \quad (125)$$

where

$$\begin{aligned} \tilde{S}_G = & +\frac{1}{2\chi_*} \int dz (n_+(z) - n_-(z))^2 \\ & +\frac{n}{\sigma_*^2} \int dz (n_+(z) + n_-(z)) \left(\log \frac{n_+(z) + n_-(z)}{n} - 1 \right). \end{aligned} \quad (126)$$

The trace (Tr_f) is in flavor space and the trace (Tr) is over flavor and Dirac indices with an integration over momentum.

• Gluonic contribution

Let us first turn our attention to the last three terms of the effective action (125).

$$\begin{aligned} S_G [P^\pm, n_\pm] = & + \int dz n_\pm(z) \text{Tr}_f \log \left(\frac{4P^\pm(z)}{n^* \rho} \right) \\ & + \int dz n_\pm(z) \log N_f! \\ & + \frac{1}{2\chi_*} \int dz (n_+(z) - n_-(z))^2 \\ & + \frac{n}{\sigma_*^2} \int dz (n_+(z) + n_-(z)) \left(\log \frac{n_+(z) + n_-(z)}{n} - 1 \right). \end{aligned} \quad (127)$$

Using the saddle approximation in the scalar glueball source $\sigma(z)$ fluctuations, we obtain

$$n_* = n \exp \left(-\frac{\sigma_*^2}{n - N_f/\sigma_*^2} \log N_f! \prod_f \frac{4P}{n\rho} \right). \quad (128)$$

As first discussed in [23] and later in [16], the distribution of the fluctuations in the number densities $n_\pm(z)$ is Gaussian (exact) in $\chi(z)$ with a width given by (6). The distribution is logarithmic in the sum $\sigma(z)$ and Gaussian (approximate) in the large N_c limit with a dispersion relation given by (7). Along with the saddle point decomposition of the bilocal auxilliary field $P^\pm = P e^{\pm i\pi_{ps}/2} (1 + \pi_s) e^{\pm i\pi_{ps}/2}$, we obtain ⁸

$$S_G [P^\pm, n_\pm] = -\frac{Nn}{\sigma_*^2} + S_G^{(1)} [\pi_{s,ps}] + S_G^{(2)} [\pi_{s,ps}, \sigma, \chi]. \quad (129)$$

⁸ This parametrization is reminiscent of the action being invariant (for massless quarks) under global axial transformation with the subscript s and ps respectively standing for the scalar and pseudoscalar mesonic excitations.

Adopting the nonet decompositions $\pi_{ps} = \lambda_0 \eta_0 + \sum \lambda_a \pi_{ps}^a$ and $\pi_s = \lambda_0 \pi_{s,0} + \sum \lambda_a \pi_s^a$, the term $S_G^{(1)} [\pi_{s,ps}]$ contains mesonic fluctuations only and reads

$$S_G^{(1)} [\pi_{s,ps}] = -\frac{n_*}{2} \int dz \text{Tr}_f \left(\pi_s^2(z) - \pi_{ps}^2(z) \right) + \int dz N_f \left(\chi_* \eta_0^2(z) - \sigma_*^2 \pi_{s,0}^2(z) \right). \tag{130}$$

We point out that the term $S_G^{(1)} [\pi_{s,ps}]$ should be put in concert with the first two terms of $S_{\text{eff}}[P^\pm, n_\pm]$ in order to obtain the total mesonic contribution to (125).

The last term $S_G^{(2)} [\pi_{s,ps}, \sigma, \chi]$ involves mixing on the one hand between the isosinglet scalar and the scalar glueballs, and, between the isosinglet pseudoscalar and the pseudoscalar glueballs, on the other hand.

$$S_G^{(2)} [\pi_{s,ps}, \sigma, \chi] = + \int dz \frac{1}{2\chi_*} \left(\chi(z) + i\chi_* \sqrt{2N_f} \eta_0(z) \right)^2 + \int dz \frac{1}{2\sigma_*^2} \left(\sigma(z) + \sigma_*^2 \sqrt{2N_f} \pi_{s,0}(z) \right)^2. \tag{131}$$

• Mesonic contribution

Performing a Taylor expansion of P^\pm around the saddle point P in the first two terms of $S_{\text{eff}}[P^\pm, n_\pm]$ (125) along with $S_G^{(1)} [\pi_{s,ps}]$ the total mesonic contribution reads⁹

$$S_{\text{meson}} [\pi_{s,ps}] = -N_c \text{Tr} \log S^{-1}(P) - 4V m_f P(m_f) - N_c \int dk \pi_s^{fg}(k) \Delta_+(k, m_f, m_g) \pi_s^{gf}(-k) + N_c \int dk \pi_{ps}^{fg}(k) \Delta_-(k, m_f, m_g) \pi_{ps}^{gf}(-k) + \int dk \left(\eta_0(k) \frac{\chi_* N_f}{N_c} \eta_0(-k) - \pi_{s0}(k) \frac{\sigma_* N_f}{N_c} \pi_{s0}(-k) \right), \tag{132}$$

where the saddle point approximation leads to an integral (gap) equation in $P(m_f)$ for each flavor f

$$\frac{4N_c}{n} \int dk A(k; M_k P(m_f); m_f) = 1 - 2m_f \frac{2P(m_f)}{n}. \tag{133}$$

⁹ The sum over flavor indices f and g is understood.

After rescaling the constituent mass according to $M_k P \rightarrow M_k$ with $P(m_f) = n\lambda(m_f)/2$, we obtain the gap equation (20) in the text. We define below the various quantities introduced in the mesonic action (132). In momentum space, we write the inverse quark propagator in the background of instantons and antiinstantons as

$$\langle k|S^{-1}(P)|l\rangle = \delta(k-l)S^{-1}(k, m) \quad (134)$$

and

$$S^{-1}(k, m) = \frac{-iM_k P}{k^2} (\not{k} - im) \left(\not{k} - i \left(\frac{k^2}{M_k P} - m \right) \right). \quad (135)$$

The coefficient $A(k; M_k; m)$ appearing in the gap equation is given by

$$A(k; M_k; m) = \frac{k^2}{M_k} \frac{M_k - m + \frac{M_k m^2}{k^2}}{k^2 + \left(m - \frac{k^2}{M_k}\right)^2}. \quad (136)$$

Except for the isosinglet scalar and pseudoscalar, the inverse meson propagator in the background of instantons and antiinstantons, apart from the factor $f^2/4N_c$, can be identified with $\Delta_{\pm}(k)$ appearing in the quadratic part of (132) and reads

$$\Delta_{\pm}(k, m_1, m_2) = \frac{n}{2N_c} - 2 \int dq (A_1 A_2 \mp (q_1 \cdot q_2) B_1 B_2). \quad (137)$$

where we have set $q_{1,2} = q \pm k/2$, $M_1 = M_{q_1}(m_1)$, $A_1 = A(q_1; M_1; m_1)$, $B_1 = B(q_1; M_1; m_1)$, m_1 being one of the quark masses in SU(3) flavor space and B is given by

$$B(k; M_k; m) = \frac{k^2}{M_k} \frac{1}{k^2 + \left(m - \frac{k^2}{M_k}\right)^2}. \quad (138)$$

In what follows, we will always consider the rescaled constituent mass $M_k(m_f)$.

- Bosonized partition function

To be thorough, let us exhibit the bosonized partition function utilized in evaluating the various (mesonic, baryonic and gluonic) correlators. To this end,

$$Z = \int \mathcal{D}\pi_{s,ps} \mathcal{D}\sigma \mathcal{D}\chi e^{-S_{\text{eff}}[\pi_{s,ps}, \sigma, \chi]}, \quad (139)$$

where the bosonized action follows from regrouping terms in S_G (129) and S_{meson} (132).

$$S_{\text{eff}}[\pi_{s,ps}, \sigma, \chi] = S_{\text{eff}}^{(0)}\left[0, \frac{n}{2}, 0\right] + S_{\text{eff}}[\pi_{s,ps}] + S_{\text{eff}}[\sigma, \chi] \tag{140}$$

with

$$S_{\text{eff}}^{(0)}\left[0, \frac{n}{2}, 0\right] = -N_c \text{Tr} \log S^{-1}(P) - \frac{Nn}{\sigma_*^2} + N \text{Tr}_f \log \frac{P}{n\rho} - 4V m_f P(m_f) \tag{141}$$

along with the mesonic part of the effective action

$$\begin{aligned} S_{\text{eff}}[\pi_{s,ps}] = & -N_c \int dk \pi_s^{fg}(k) \Delta_+(k, m_f, m_g) \pi_s^{gf}(-k) \\ & + N_c \int dk \pi_{ps}^{fg}(k) \Delta_-(k, m_f, m_g) \pi_{ps}^{gf}(-k) \\ & + \int dk \left(\eta_0(k) \frac{\chi_* N_f}{N_c} \eta_0(-k) - \pi_{s0}(k) \frac{\sigma_* N_f}{N_c} \pi_{s0}(-k) \right) \end{aligned} \tag{142}$$

and the gluonic part of the effective action

$$\begin{aligned} S_{\text{eff}}[\sigma, \chi] = & + \int dz \frac{1}{2\chi_*} \left(\chi(z) + i\chi_* \sqrt{2N_f} \eta_0(z) \right)^2 \\ & + \int dz \frac{1}{2\sigma_*^2} \left(\sigma(z) + \sigma_* \sqrt{2N_f} \pi_{s,0}(z) \right)^2. \end{aligned} \tag{143}$$

We are now in a position to evaluate the correlation functions of interest.

• Connected meson correlator

From the expression of $C_\gamma^0(x)$ (35) in the text along with the bosonized partition function (139), we easily find that to leading order in N_c (the trace being over flavor as well as Dirac indices)

$$C_\gamma^0(x) = -N_c \text{Tr} \left(S(x, m) \gamma S(-x, m) \gamma \right) \tag{144}$$

along with its p -space version $C_\gamma^0(p)$ quoted in (37) of the main text.

• Unconnected meson correlator

From the expression of $C_\gamma^1(x)$ (36) in the text, we need to examine the term $\text{Tr } \gamma S(x, x, P^\pm)$ in the integrand (the trace being in flavor, color and Dirac space). With the shorthand notation

$$\tilde{\pi} = \pi_s - \frac{\pi_{ps}^2}{2} + i\gamma_5 \left(\pi_{ps} + \frac{1}{2}\pi_s\pi_{ps} + \frac{1}{2}\pi_{ps}\pi_s \right) \quad (145)$$

we can write

$$\text{Tr } \gamma S(x, x, P^\pm) = \int dk dl e^{i(k-l)x} \text{Tr } \gamma S(k, l, P^\pm), \quad (146)$$

where the relevant term in the large N_c limit is given according to

$$\begin{aligned} S(k, l, P^\pm) &= S(k, m) \delta(k-l) + i\sqrt{M_k} C(k, m) \tilde{\pi}(k-l) C(l, m) \sqrt{M_l} \\ &\quad - \sqrt{M_k} C(k, m) \left(\int dq \tilde{\pi}(k-q) \sqrt{M_q} \left(1 - \frac{imq}{q^2} \right) \right. \\ &\quad \left. \times S(q, m) \left(1 - \frac{imq}{q^2} \right) \sqrt{M_q} \tilde{\pi}(q-l) \right) C(l, m) \sqrt{M_l}. \end{aligned} \quad (147)$$

The coefficient $C(k, m)$ is given further below. Defining

$$C_\gamma^1(p, q) = \delta(p-q) \left(\tilde{C}_\gamma^1(p) + C_\gamma^{1'}(p) \right), \quad (148)$$

where

$$\begin{aligned} \tilde{C}_\gamma^1(p) &= -\frac{\delta(p)}{Z} \int \mathcal{D}\pi_{s,ps} \mathcal{D}\sigma \mathcal{D}\chi \exp(-S_{\text{eff}}[\pi_{s,ps}, \sigma, \chi]) \\ &\quad \times \text{Tr } \gamma S \left(\text{Tr } \gamma S - 2\text{Tr } \gamma \sqrt{M_k} C \tilde{\pi} (B\hat{k} + iA) \tilde{\pi} C \sqrt{M_l} \right). \end{aligned} \quad (149)$$

Here, the trace carries an integral over momentum. The meson field $\tilde{\pi}$ is left inside the trace so as to reflect its bilocal character in the momentum. It is clear that $\tilde{C}_\gamma^1(p)$ vanishes identically except in the isoscalar singlet $\pi_{s,0}$. From a diagram approach, it has two unconnected closed fermion loops with possibly the $\pi_{s,0}$ being emitted within one loop (Fig. 3(c)). Further discussion will be presented in the text regarding this term.

We are therefore left with the second term contribution in $C_\gamma^1(p)$. This term amounts to a propagating meson from one closed fermion loop to the

other (Fig. 3(d)) and reads

$$C_\gamma^1(p) = -\frac{N_c}{Z} \int \mathcal{D}\pi_{s,ps} \mathcal{D}\sigma \mathcal{D}\chi R_\gamma(p, m_f, m_g) R_\gamma(-p, m_f, m_g) \times \exp\left(-S_{\text{eff}}[\pi_{s,ps}, \sigma, \chi]\right), \tag{150}$$

where

$$R_\gamma(p, m_f, m_g) = \int dk \sqrt{M_1 M_2} \text{Tr}\left(\gamma C(k_1, m_f) \tilde{\pi}(p) C(k_2, m_g)\right) \tag{151}$$

with $k_{1,2} = k \pm p/2$, $M_1 = M_{k_1}(m_f)$ and

$$C(k, m) = S(k, m) \left(1 - \frac{im\not{k}}{k^2}\right). \tag{152}$$

If we redefine R_γ so as to extract the meson field, we have

$$R_\gamma(p, m_f, m_g) = R_\gamma^\pm(p, m_f, m_g) \pm R_\gamma^\mp(p, m_f, m_g) \tag{153}$$

with

$$R_\gamma^\pm(p, m_{1,2}) = \int \frac{d^4k}{(2\pi)^4} \sqrt{M_1 M_2} \text{Tr}\left(\gamma C_1 \frac{1 \pm \gamma_5}{2} C_2\right) \tag{154}$$

and

$$C_{1,2} = \frac{\not{k}_{1,2}}{k_{1,2}^2} (1 - A_{1,2}) + iB_{1,2}. \tag{155}$$

Performing the functional integral, we obtain (38). As an example, we exhibit the case of the mixing singlet η_0 and octet η_8 . The specific flavor character of R_γ^\pm follows from the effective action (142) for the nonet decomposition. For instance, the pertinent terms R_{γ_5} (151) for the η_0 and η_8 correlators are given by

$$\int dk \sqrt{M_1 M_2} \text{Tr}_f (\gamma_5 \lambda_{0,8} C(k_1, m) \gamma_5 C(k_2, m) \kappa(p)). \tag{156}$$

Explicitly, for the unconnected parts of the η_0 and η_8 correlators, we obtain

$$C_{\eta_{0,8}}^1(p) = -\frac{N_c}{Z} \int \mathcal{D}\eta_{0,8} \tilde{\mathbf{R}}_{0,8}(-p) \boldsymbol{\eta}(-p) \tilde{\boldsymbol{\eta}}(p) \mathbf{R}_{0,8}(p) e^{N_c \int \tilde{\boldsymbol{\eta}}[\boldsymbol{\Delta}]\boldsymbol{\eta}}, \tag{157}$$

where the partition function Z in the denominator contains only η_0 and η_8 . For the η_0 we have

$$\mathbf{R}_0(p) = \begin{pmatrix} \frac{4}{3}R(p) + \frac{2}{3}R_s(p) \\ \frac{2\sqrt{2}}{3}(R(p) - R_s(p)) \end{pmatrix} \quad (158)$$

and for the η_8

$$\mathbf{R}_8(p) = \begin{pmatrix} \frac{2\sqrt{2}}{3}(R(p) - R_s(p)) \\ \frac{2}{3}R(p) + \frac{4}{3}R_s(p) \end{pmatrix} \quad (159)$$

with $R(p) = R_{\gamma_5}(p, m)$ and similarly $R_s(p) = R_{\gamma_5}(p, m_s)$ where m and m_s are the up (down) and strange quark mass respectively (151).

$$C_{\eta_{0,8}}^1(p) = \frac{N_c}{2} \tilde{\mathbf{R}}_{0,8}(-p) [\Delta(p)]^{-1} \mathbf{R}_{0,8}(p). \quad (160)$$

Appendix D

Nonet decomposition

Taking the partition function (139) derived for $N_f > 1$ with the same decomposition for the meson fields $\pi_{s,ps}$, we have as the mesonic effective action (142)

$$\begin{aligned} S_{\text{eff}}[\pi_{s,ps}] = & -N_c \int dk \pi_s^{fg}(k) \Delta_+(k, m_f, m_g) \pi_s^{gf}(-k) \\ & + N_c \int dk \pi_{ps}^{fg}(k) \Delta_-(k, m_f, m_g) \pi_{ps}^{gf}(-k) \\ & + \int dk \left(\eta_0(k) \frac{\chi_* N_f}{N_c} \eta_0(-k) - \pi_{s0}(k) \frac{\sigma_* N_f}{N_c} \pi_{s0}(-k) \right), \end{aligned} \quad (161)$$

where f and g are flavor labels (f is not to be confused with the pseudoscalar decay constant). Using the decomposition $\pi_{ps} = \sum_{k=0}^8 \kappa_k \lambda_k$, the κ_0 and κ_8 excitations contribute to S_{eff} in the form

$$S_{\text{eff}}[\eta_0, \eta_8] = N_c \int dk \tilde{\eta}(k) [\Delta(k)] \eta(-k), \quad (162)$$

where $\tilde{\eta}(p) = (\eta_0(p), \eta_8(p)) = f(\kappa_0(p), \kappa_8(p))$ and

$$[\mathbf{\Delta}(k)] = \begin{pmatrix} \frac{2}{3}(2\Delta + \Delta_s) + \frac{\chi_* N_f}{N_c} & \frac{2\sqrt{2}}{3}(\Delta - \Delta_s) \\ \frac{2\sqrt{2}}{3}(\Delta - \Delta_s) & \frac{2}{3}(\Delta + 2\Delta_s) \end{pmatrix} \quad (163)$$

with the shorthand notation $\Delta = \Delta(k, m, m)$ $\Delta_s = \Delta(k, m_s, m_s)$ with the strange quark mass inserted. The contribution $\chi_* N_f / N_c$ follows from the singlet mixing with the topological fluctuations through the measure (5). At low energy, and to leading order in the current mass

$$\begin{aligned} S_{\text{eff}}[\eta_0, \eta_8] &= + \int dk \frac{1}{2} f^2 k^2 (\eta_0^2 + \eta_8^2) + \int \frac{1}{2} (2N_F \chi_*) \eta_0^2 \\ &\quad - \int dk \frac{1}{2} \langle \bar{\psi} \psi \rangle \left(\eta_0^2 \left(\frac{4}{3}m + \frac{2}{3}m_s \right) + \eta_8^2 \left(\frac{2}{3}m + \frac{4}{3}m_s \right) \right) \\ &\quad - \int dk \frac{1}{2} \langle \bar{\psi} \psi \rangle \eta_0 \eta_8 \frac{4\sqrt{2}}{3} (m_s - m). \end{aligned} \quad (164)$$

Note that $S_{\text{eff}}[\eta_0, \eta_8] \sim N_c$. The above result yields the GOR relations for the singlet and the octet, if we were to drop $\frac{nN_f}{N_c}$. As is well known, the GOR result is badly violated in the singlet channel by the axial U(1) anomaly. The latter is carried over by local fluctuations in the topological charge, which results in a mixing with the singlet quantum numbers as displayed in (164).

Appendix E

Extended bosonization

The use of the mean-field equation (109) in Appendix A has allowed for a bosonization scheme that is trouble free. Indeed, if we were to carry a gaussian analysis around all the fields *including* the auxillary field π^\pm , and hence expand (109), then instabilities show up along the scalar (π_s) and pseudoscalar (π_{ps}) directions. This, however, can be easily fixed through a generalization of (13) to include fluctuations around the instanton densities. We start with a modification in (13)

$$\mathbf{1} = \int \mathcal{D}\pi^\pm \mathcal{D}P^\pm \exp \left(\text{Tr}_f \int dz P^\pm(z) \left(\pi^\pm(z) - \frac{N^\pm(z)}{n^*/2} \theta^\pm(z) \right) \right) \quad (165)$$

that is inserted in the partition function (2), where the term in the exponent

$$\frac{N^\pm(z)}{n^*/2} = 1 + \frac{g_s \sigma(z) + g_{ps} \chi(z)}{n^*} \quad (166)$$

clearly couples scalar (pseudoscalar) glueballs to the quarks with strength g_s (g_{ps}) (see (169) below).

Following the steps of Appendix C, the mean field equation in π^\pm reads

$$-iP^\pm(z) = \frac{n^*}{4im} \frac{n^\pm(z)}{N^\pm(z)} \frac{1}{1 - n^* \pi^\pm(z)/(4im N^\pm(z))}. \quad (167)$$

Along with the contribution from the measure $\mu(n_+, n_-)$ (5) the bosonized effective action reads

$$\begin{aligned} S_{\text{eff}} = & -N_c \text{Tr} \log \mathbf{S}^{-1}[P^\pm, \sigma, \chi] - 2 \int dz \frac{N^\pm(z)}{n^*/2} \text{Tr}_f m P^\pm(z) \\ & + \int dz n_\pm(z) \log \left(N_f! \prod_f \frac{4P^\pm(z) N^\pm(z)}{n^* \rho n^\pm(z)} \right) \\ & + N_f \int dz \left(n^+(z) + n^-(z) \right) + \tilde{S}_G, \end{aligned} \quad (168)$$

where \tilde{S}_G is the gluonic contribution (126). The inverse quark propagator $\mathbf{S}^{-1}[P^\pm, \sigma, \chi]$ in (168) is

$$\begin{aligned} \mathbf{S}^{-1}[P^\pm, \sigma, \chi] = & +\mathbf{S}^{-1}[P^+, P^-] \\ & -i\sqrt{M_k} \left(1 - \frac{im\hat{k}}{k^2} \right) \frac{g_s \sigma(z) + g_{ps} \chi(z)}{n^*} \\ & \times \left(1 + \pi_s + i\gamma_5 \pi_{ps} \right) \left(1 - \frac{im\hat{k}}{k^2} \right) \sqrt{M_k} \end{aligned} \quad (169)$$

and its second term clearly exhibits glueballs coupling to quarks. The first term $\mathbf{S}^{-1}[P^+, P^-]$ in (169) is given in (17). Following the saddle point approximation used in Appendix C, we obtain the effective action as follows

$$\begin{aligned} S_{\text{eff}}[\pi_s, \pi_{ps}, \sigma, \chi] = & -N_c \text{Tr} \log S^{-1}(P) + n^* V \left(N_f - \text{Tr}_f \frac{4mP}{n^*} - \frac{n}{\sigma_*} \right) \\ & - N_c \int dk \pi_s^{fg}(k) \Delta_+(k, m_f, m_g) \pi_s^{gf}(-k) \\ & + N_c \int dk \pi_{ps}^{fg}(k) \Delta_-(k, m_f, m_g) \pi_{ps}^{gf}(-k) \\ & + S_{\text{eff}}[\sigma^2, \sigma, \pi_s] \\ & + S_{\text{eff}}[\chi^2, \chi, \pi_{ps}]. \end{aligned} \quad (170)$$

In the last two terms of (170), we have lumped terms in σ^2 , $\sigma\pi_s$, χ^2 and $\chi\pi_{ps}$ where π_s (π_{ps}) is decomposed in the scalar (pseudoscalar) unphysical

basis (in flavor space) π_s^{fg} (π_{ps}^{fg}). Only diagonal terms π_s^{ff} (π_{ps}^{ff}) mix with scalar (pseudoscalar) glueballs according to

$$\begin{aligned} S_{\text{eff}}[\sigma^2, \sigma \pi_s] = & + \int dk \sigma(k) g_s^\sigma(k) \sigma(-k) \\ & + \int dk \sigma(k) \sum_f \left(1 - g_s \frac{2N_c}{n_*} \Delta_+(k, m_f, m_f) \right) \pi_s^{ff}(-k), \end{aligned} \quad (171)$$

where

$$g_s^\sigma(k) = \frac{n}{2n_* \sigma_*^2} + \frac{g_s^2}{2n_*} \sum_f \left(1 - \frac{2N_c}{n_* N_f} \Delta_+(k, m_f, m_f) \right) - \frac{N_f}{2n_*} (g_s - 1)^2. \quad (172)$$

The point made at the start of this Appendix can now be appreciated. We see that if we set $g_s = 0$ the result differs from what we had in Appendix C by the last term. The latter with its negative sign can cause an instability in the scalar glueball fluctuations. This is easily tamed by the use of the bosonization scheme discussed in Appendix C.

For the pseudoscalar part, we have

$$\begin{aligned} S_{\text{eff}}[\chi^2, \chi \pi_{ps}] = & + \int dk \chi(k) g_{ps}^\chi(k) \chi(-k) \\ & + \int dk \chi(k) \sum_f \left(1 - g_{ps} \frac{2N_c}{n_*} \Delta_-(k, m_f, m_f) \right) i\pi_{ps}^{ff}(-k), \end{aligned} \quad (173)$$

where

$$g_{ps}^\chi(k) = \frac{1}{2\chi_*} + \frac{g_{ps}^2}{2n_*} \sum_f \left(1 - \frac{2N_c}{n_* N_f} \Delta_-(k, m_f, m_f) \right) - \frac{N_f}{2n_*} (g_{ps} - 1)^2. \quad (174)$$

Again, if $g_{ps}=0$ the latter term may cause the fluctuations in the pseudoscalar glueball direction to be unstable. This is easily tamed by the bosonization scheme discussed in Appendix C.

As a check, we clearly see that in the absence of fermion we recover the scalar (pseudoscalar) gluonic contribution \tilde{S}_G for $n_\pm = (n + \sigma \pm \chi)/2$. The expression (171) in terms of physical scalar meson field in λ_0 and λ_8 channels (flavor space) reads

$$\begin{aligned} S_{\text{eff}}[\sigma^2, \sigma \pi_s] = & + \int dk \sigma(k) g_s^\sigma(k) \sigma(-k) \\ & + \int dk \sigma(k) \sqrt{2N_f} \left(g_s^0(k) \pi_{s0}(-k) + g_s^8(k) \pi_{s8}(-k) \right) \end{aligned} \quad (175)$$

and similarly (173) for the pseudoscalar sector reads

$$S_{\text{eff}}[\chi^2, \chi \pi_{ps}] = + \int dk \chi(k) g_{ps}^\chi(k) \chi(-k) + \int dk \chi(k) i\sqrt{2N_f} \left(g_{ps}^0(k) \eta_0(-k) + g_{ps}^8(k) \eta_8(-k) \right). \quad (176)$$

We have defined above for the scalar (pseudoscalar) part of the action

$$g_{s,ps}^0(k) = 1 - g_{s,ps} \frac{2N_c}{n_* N_f} \left(2\Delta_\pm(k, m, m) + \Delta_\pm(k, m_s, m_s) \right), \quad (177)$$

$$g_{s,ps}^8(k) = g_{s,ps} \frac{2N_c}{n_* N_f} \sqrt{2} \left(\Delta_\pm(k, m_s, m_s) - \Delta_\pm(k, m, m) \right). \quad (178)$$

The expression of n_* and the mass gap equation of Appendix C remain unchanged.

• Scalar gluonic correlator $C_{FF}(x, y)$

The form of the scalar gluonic correlator is unchanged up to a constant term

$$C_{FF}(x - y) = \int dk e^{ik(x-y)} \left(\frac{n}{n_* \sigma_*^2} + \frac{1}{2N_c} \sum_{f=1}^{N_f} \left(\frac{1}{\Delta_+(k, m_f, m_f)} - \frac{2N_c}{n_*} \right) \right)^{-1}. \quad (179)$$

• Pseudoscalar gluonic correlator $C_{FF}(x, y)$

Similarly, for the pseudoscalar gluonic correlator

$$C_{F\tilde{F}}(x - y) = \int dk e^{ik(x-y)} \left(\frac{1}{\chi_*} + \frac{1}{2N_c} \sum_{f=1}^{N_f} \left(\frac{1}{\Delta_-(k, m_f, m_f)} - \frac{2N_c}{n_*} \right) \right)^{-1}. \quad (180)$$

• Pseudoscalar form factor

For the pseudoscalar case, we have

$$F_p(0) = \frac{32\pi^2}{2N_c \Delta_-(0, m, m)} \left(\frac{1}{\chi_*} + \frac{1}{2N_c} \sum_f \left(\frac{1}{\Delta_-(0, m_f, m_f)} - \frac{2N_c}{n_*} \right) \right)^{-1} \quad (181)$$

as indicated in Section 8.

- Scalar form factor

For the scalar case, we have

$$F_s(0) = \frac{32\pi^2}{2N_c\Delta_+(0, m, m)} \left(\frac{n}{n_*\sigma_*^2} + \frac{1}{2N_c} \sum_f \left(\frac{1}{\Delta_+(0, m_f, m_f)} - \frac{2N_c}{n_*} \right) \right)^{-1} \quad (182)$$

as indicated in Section 8.

- Pseudoscalar coupling constant g_{ps}

In order to determine the strength $g_{ps}(k=0)$ of the pseudoscalar glueballs coupling constant to the quarks, we fit the experimental value of the mixing angle $\theta = -20^\circ$ when diagonalizing. The result gives an estimate for g_{ps} ($k=0$ is understood) according to

$$\begin{aligned} 2 \cot 2\theta & \left(\frac{2\sqrt{2}}{3} g_{ps}^\chi (\Delta - \Delta_s) + \frac{N_f}{2} g_{ps}^0 g_{ps}^8 \right) \\ & = \frac{2}{3} g_{ps}^\chi (\Delta - \Delta_s) + \frac{N_f}{2} (g_{ps}^{0^2} - g_{ps}^8) . \end{aligned} \quad (183)$$

We obtain $g_{ps} = -7.025$.

Appendix F

Unconnected correlators

We tabulate below the expressions for the unconnected correlator $C_\gamma^1(p)$ in the various channels

γ	$\text{Tr} \left(\gamma \mathbf{C}_1 \frac{1+\gamma_5}{2} \mathbf{C}_2 \right)$	$\mathbf{C}_\gamma^1(p) / 2N_c$
1	$2 \left((1 - A_1) (1 - A_2) \frac{k_1 k_2}{k_1^2 k_2^2} - B_1 B_2 \right)$	$\frac{(R_1^+(p))^2}{\Delta_+(p)}$
γ_5	$-2 \left((1 - A_1) (1 - A_2) \frac{k_1 k_2}{k_1^2 k_2^2} + B_1 B_2 \right)$	$\frac{(R_{\gamma_5}^+(p))^2}{\Delta_-(p)}$
γ_μ	$2 \left(\frac{kx+p/2}{k_1^2} (1 - A_1) B_2 + \frac{kx-p/2}{k_2^2} (1 - A_2) B_1 \right)$	$\frac{(R_\mu^+(p))^2}{\Delta_+(p)}$
$\gamma_5 \gamma_\mu$	$2 \left(\frac{kx+p/2}{k_1^2} (1 - A_1) B_2 - \frac{kx-p/2}{k_2^2} (1 - A_2) B_1 \right)$	$\frac{(R_{\gamma_5 \gamma_\mu}^+(p))^2}{\Delta_-(p)}$
$\sigma_{\mu\nu}$	$R_\pm^{\mu\nu}(p) = 0$	0

Appendix G

m_s expansion

In this Appendix, we give the details leading to (39). Inserting the mass gap equation for small quark masses m_1 and m_2 in the first term of $\Delta_{\pm}(p, m, m)$ with the following approximations

$$A \simeq \frac{M^2 - mM}{k^2 + M^2 - 2mM}, \quad B \simeq \frac{M}{k^2 + M^2 - 2mM} \quad (184)$$

we obtain (denoting $\Delta_{\pm}(p) = \Delta_{\pm}(p, m, m)$)

$$\begin{aligned} \Delta_{\pm}(p) &= \frac{n}{2N_c} (m_1 \lambda_1 + m_2 \lambda_2) + \int \frac{d^4 k}{(2\pi)^4} \frac{(k_1 M_2 \pm k_2 M_1)}{(k_1^2 + M_1^2)(k_2^2 + M_2^2)} \\ &\quad - (m_1 + m_2) \int \frac{d^4 k}{(2\pi)^4} \frac{M_k^4 + k^4 - 2M_k^2 k^2 \mp 4M_k^2 k^2}{(k^2 + M_k^2)^3}. \end{aligned} \quad (185)$$

At small momentum, and using

$$(k_1 M_2 - k_2 M_1)^2 = p^2 M_k^2 + (k \cdot p)^2 (M_k'^2 - 2M_k M_k'/k),$$

we obtain

$$\begin{aligned} \Delta_{\pm}(p) &= p^2 \int \frac{d^4 k}{(2\pi)^4} \frac{(M_k^2 - k M_k M_k'/2 + k^2 M_k'^2/4)}{(k^2 + M_k^2)^2} \\ &\quad + \frac{n}{2N_c} (m_1 \lambda_1 + m_2 \lambda_2) - (m_1 + m_2) \int \frac{d^4 k}{(2\pi)^4} \frac{M_k}{k^2 + M_k^2}, \end{aligned} \quad (186)$$

To illustrate the fact that the approximations used for A and B fail in the case of a strange quark mass, we show the plots of A (Fig. 23) and B (Fig. 24) for both the up (a) and strange quark (b). The solid line is the unexpanded result, while the dotted line is the expanded one.

Appendix H

Outline of the numerics

In this Appendix, we sketch how the numerical calculations were performed. First, we solve the integral equation (20) for $\lambda(m)$. With the constituent mass $M_k(m)$ fully known (41), the propagator $S(x, m)$ follows.

The decomposition (24) of $S(x, m)$ lends itself to a straightforward numerical integration of $S_1(x, m)$ (27), (28). The singular behavior at $x = 0$ is contained in $S_0(x, m)$. In p -space, each correlator is the sum of an connected part (37) and a unconnected part (38). To speed up the convergence of the numerical integration of (37), the free bubble diagram is removed by hand and later added. The evaluation of (38) is achieved in stages (numerator and denominator). Because we will later on numerically Fourier transform the p -space version of (38), great care is taken at low momenta since the reading of a meson mass is done at large distance. In x -space, the connected part of each correlator is directly evaluated from the x -space version of the propagator $S(x, m)$ as

$$C_\gamma^0(x) = -N_c \text{Tr}(S(x, m)\gamma S(-x, m)\gamma). \quad (187)$$

For the unconnected correlator, we numerically Fourier transform its p -space version. In the pion case, we sum the two parts of the correlator and read the pion mass from the large distance behavior of $x^{3/2}$ times the correlator. The kaon unconnected correlator is exponentially damped by a factor of $m_\pi - m_K$ with its pion analog and turns out to be of about the same order as its connected part. Therefore, we single out the unconnected part to read the kaon mass.

REFERENCES

- [1] A. Di Giacomo, *Nucl. Phys.* **B23**, 191 (1991); O. Miyamura, S. Origuchi, Hiroshima preprint 95-08.
- [2] C.G. Callan, R.F. Dashen, D.J. Gross *Phys. Rev.* **D19**, 1826 (1979).
- [3] M.-C. Chu, J.M. Grandy, S. Huang, J. W. Negele, *Phys. Rev. Lett.* **70**, 225 (1993).
- [4] M. -C. Chu, J.M. Grandy, S. Huang, J.W. Negele, *Phys. Rev.* **D48**, 3340 (1993).
- [5] M. Tepper, *Nucl. Phys.* **B411**, 855 (1994).
- [6] J. Polonyi, *Phys. Rev.* **D29**, 716 (1984).
- [7] H. Yamagishi, I. Zahed, Stony Brook preprint SUNY-NTG-95/29 (1995).
- [8] E.V. Shuryak, J.J.M. Verbaarschot, *Nucl. Phys.* **B410**, 37,55 (1993).
- [9] G. 't Hooft, *Phys. Rev. Lett.* **37**, 8 (1976); *Phys. Rev.* **D14**, 3432 (1976); *Phys. Rev.* **D18**, 2199 (1978); *Phys. Rep.* **142**, 357 (1986).
- [10] E.V. Shuryak, *Nucl. Phys.* **B203**, 116, 140, 237 (1982); *Nucl. Phys.* **B214**, 237 (1983).
- [11] M. Chemtob, *Physica Scripta* **29**, 17 (1984).

- [12] D.I. Dyakonov, V.Yu. Petrov, *Phys. Lett.* **B147**, 351 (1984); *Sov. Phys. JETP* **62**, 204 (1985).
- [13] D.I. Dyakonov, V.Yu. Petrov, *Nucl. Phys.* **B272**, 457 (1986).
- [14] E.V. Shuryak *Nucl. Phys.* **302**, 559, 574, 599, 621 (1988); *Nucl. Phys.* **319**, 521, 541 (1989).
- [15] D.I. Dyakonov, V.Yu. Petrov, Leningrad preprint LNPI-1153,1986.
- [16] M.A. Nowak, J.J.M. Verbaarschot, I. Zahed, *Phys. Lett.* **B228**, 251 (1989).
- [17] R. Alkofer, M.A. Nowak, J.J.M. Verbaarschot, I. Zahed, *Phys. Lett.* **B233**, 205 (1989).
- [18] M.A. Nowak, J.J.M. Verbaarschot, I. Zahed, *Phys. Lett.* **B226**, 382 (1989).
- [19] M.A. Nowak, J.J.M. Verbaarschot, I. Zahed, *Nucl. Phys.* **B324**, 1 (1989).
- [20] M.A. Nowak, *Acta Phys. Pol.* **22**, 697 (1991).
- [21] I. Zahed, *Nucl. Phys.* **B427**, 561 (1994).
- [22] E.V. Shuryak, J.J.M. Verbaarschot, *Phys. Rev.* **D52**, 295 (1995).
- [23] D.I. Dyakonov, V.Yu. Petrov, *Nucl. Phys.* **B245**, 259 (1984).
- [24] J.J.M. Verbaarschot, *Nucl. Phys.* **B362**, 33 (1991); *Nucl. Phys.* **B386**, 236 (1992).
- [25] E. Witten, *Nucl. Phys.* **B156**, 269 (1979).
- [26] V.A. Novikov, M.A. Shifman, A.I. Vainshtein, V.I. Zakharov, *Phys. Rep.* **116**, 103 (1984).
- [27] D.I. Dyakonov, V.Yu. Petrov, *Quark Cluster Dynamics in Lecture Notes in Physics* **417**, Springer-Verlag, 1992, p.288.
- [28] S.V. Esaibegian, S.N. Tamarian, *Sov. J. Nucl. Phys.* **49**, 507 (1989).
- [29] A.V. Radyushkin, *Phys. Lett.* **B271**, 218 (1991).
- [30] S. Chernyshev, M.A. Nowak, I. Zahed, *Phys. Lett.* **B350**, 238 (1995).
- [31] M.B. Einhorn, *Phys. Rev.* **D14**, 3451 (1976).
- [32] M. Gell-Mann, R.J. Oakes, B. Renner, *Phys. Rev.* **175**, 2195 (1968).
- [33] G. Veneziano, *Nucl. Phys.* **B159**, 461 (1979).
- [34] T. Schaefer, E.V. Shuryak, *Phys. Rev.* **D50**, 478 (1994).
- [35] M. Hutter, Munich University preprint, LMU-95-01, 1994.
- [36] E. V. Shuryak, *Rev. Mod. Phys.* **65**, 1 (1993).
- [37] D.I. Diakonov, M.V. Polyakov, C. Weiss, *Nucl. Phys.* **B461**, 539 (1996).
- [38] G. Veneziano, *Mod. Phys. Lett.* **A17**, 1605 (1989).
- [39] T. Hatsuda, I. Zahed, *Phys. Lett.* **B221**, 173 (1989).
- [40] T.P. Cheng, L.-F. Li, *Phys. Rev. Lett.* **62**, 1441 (1989).
- [41] G.M. Shore, G. Veneziano, *Phys. Lett.* **B244**, 75 (1990).
- [42] A.V. Efremov, J. Soffer, N.A. Tornqvist, *Phys. Rev.* **D44**, 1369 (1991).
- [43] J. Schechter, V. Soni, A. Subbaraman, H. Weigel, *Mod. Phys. Lett.* **A30**, 2543 (1990).

- [44] M. Wakamatsu, *Phys. Lett.* **B280**, 97 (1992).
- [45] A. Blotz, M.V. Polyakov, K. Goeke, *Phys. Lett.* **B302**, 151 (1993).
- [46] H.-Y. Cheng, Institute of Physics, Academia Sinica (ROC) preprint IP-ASTP-21-95.
- [47] D.I. Dyakonov, V.Yu. Petrov, P.V. Pobylitsa, *Phys. Lett.* **B205**, 372 (1988).
- [48] D.I. Dyakonov, V.Yu. Petrov, *Nucl. Phys.* **B323**, 53 (1989).
- [49] L.Ya. Glozman, D.O. Riska, The Baryon Spectrum and Chiral Dynamics, *pi N Newslett.* No 10, 115 (1995); Systematics of the Light and Strange Baryons and the Symmetries of QCD, preprint HU-TFT-94-48, [LANL hep-ph 9412231] (1994); *Phys. Rep.* **268**, 263 (1996).
- [50] B.L. Ioffe, *Nucl. Phys.* **B188**, 317 (1981).
- [51] P.V. Pobylitsa, *Phys. Lett.* **B226**, 387 (1989).